GROUND TEMPERATURE AND CLIMATE CHANGE

by

Michael Gregory Davis

A dissertation submitted to the faculty of
The University of Utah
in partial fulfillment of the requirements for the degree of

Doctor of Philosophy

in

Geophysics

Department of Geology and Geophysics

The University of Utah

August 2013

The University of Utah Graduate School

STATEMENT OF DISSERTATION APPROVAL

The dissertation of Michael Gregory Davis

has been approved by the following supervisory committee members:

David S. Chapman	, Chair	May 22, 2013 Date Approved
David R. Bowling	, Member	May 21, 2013 Date Approved
John R. Bowman	, Member	May 22, 2013 Date Approved
Robert N. Harris	, Member	May 22, 2013 Date Approved
D. Kip Solomon	, Member	May 23, 2013 Date Approved

and by D. Kip Solomon , Chair of

the Department of Geology and Geophysics

and by Donna M. White, Interim Dean of The Graduate School.

ABSTRACT

Three studies are presented dealing with the relationship between ground temperatures, surface meteorological parameters, and different vegetation cover. These observations are related to borehole temperature profiles and the record they provide of climate change at the decadal to centennial time scale.

The first study examines how borehole temperatures respond to surface temperature changes using three boreholes in northwestern Utah that have been repeatedly logged for temperature over a period of 29 years. Systematic subsurface temperature changes of up to 0.6 °C are observed in the upper sections of these boreholes. Synthetic temperature profiles computed from surface data at nearby meteorological stations reproduce both the amplitude and pattern of the transient temperature observations, fitting observations to within 0.03 °C or better. This provides observational confirmation of the strong coupling between surface temperature change and borehole temperature transients.

The second study compares observations from a set of meteorological stations in the Cascades Mountains in Oregon that show vegetation cover can significantly affect ground temperatures due primarily to the influence of trees shading the ground from incoming solar radiation. During the period between 2000 and 2004, air temperature differences between the two sites decreased only slightly from 1.7 °C to 1.1 °C, while ground temperature differences were cut nearly in half from 2.8 °C to 1.5 °C. These

changes are directly connected to the decrease in solar radiation over the study period as the forest grew back. Subsurface temperatures are reproducible using the Noah land surface model, but are largely influenced by incoming solar radiation.

The third section addresses the importance of public and educational outreach in the realm of climate change, which led to the development and publishing of meteorological and subsurface data from the Emigrant Pass Observatory located in the Grouse Creek Mountains in northwestern Utah through a website. The primary goals of this website are to provide a tutorial for understanding both local climate and climate change, and their relation to diffusion of temperatures into the Earth's subsurface, to facilitate access to available climate data, and to provide educational lesson ideas for using real data to understand local climate change.

TABLE OF CONTENTS

ABSTRACT.....iii

LIST OF TABLES.....vii

LIST OF FIGURES.....viii

PREFACE.....x

CHAPTER

1. REPEAT TEMPERATURE MEASUREMENTS IN BOREHOLES FROM NORTHWESTERN UTAH LINK GROUND AND AIR TEMPERATURE CHANGES AT THE DECADAL TIME SCALE.....1

    Abstract.....1
    Introduction.....2
    Borehole Temperature-Depth Profiles.....6
    Surface Air Temperature Records.....21
    Temporal Changes in Subsurface Temperature.....22
    Discussion.....31
    Conclusions.....33
    Acknowledgments.....34
    References.....34

2. SUBSURFACE THERMAL AND HYDROLOGICAL CHANGES BETWEEN A FORESTED AND A CLEAR-CUT SITE IN THE OREGON CASCADES.....37

    Abstract.....37
    Introduction.....38
    Field Site.....41
    Site Comparisons.....44
        Soapgrass Mountain Open Area.....44
        Soapgrass Mountain Mature Forest.....50
        Comparison of Soapgrass Mountain sites.....54
    Land Surface Modeling.....60
        Modeling Results and Comparisons.....63
    Discussion.....70
    Conclusions.....72
    References.....74

3. A WEB-BASED RESOURCE FOR INVESTIGATING ENVIRONMENTAL CHANGE: THE EMIGRANT PASS OBSERVATORY.....78

Abstract.....78
Introduction.....79
Emigrant Pass Observatory.....80
Use of EPO and Boreholes to Study Climate.....82
Data Products.....89
Lesson Ideas.....94
Outreach.....95
Summary.....96
References.....96

LIST OF TABLES

Table		Page
1-1.	Geothermal information for borehole sites	9
1-2.	Logging years and numbers of borehole logs used in analysis	10
1-3.	Amplitude of temperature changes between 1978 and 2007	18
1-4.	POM and thermal diffusivity for synthetic temperature calculations	25
1-5.	Amplitude of the best-fitting SAT trend	29
2-1.	Listing of weather and soil sensors at Soapgrass Mountain	45
2-2.	Annual averages of meteorological and subsurface data at the Soapgrass Mountain Open Area	47
2-3.	Annual averages of meteorological and subsurface data at the Soapgrass Mountain Mature Forest	52
2-4.	Differences between meteorological and subsurface observations at Soapgrass Mountain Open Area and Mature Forest (SMOA – SMMF)	57
2-5.	Soil and vegetation parameters at Soapgrass Mountain	63
3-1.	Available sensors at EPO	90

LIST OF FIGURES

Figure		Page
1-1.	Location map of northwestern Utah, USA, showing borehole sites	7
1-2.	Temperature-depth profiles collected between 1978 and 2007	12
1-3.	Reduced temperatures for boreholes	14
1-4.	Temperatures differences relative to the 1978 log	20
1-5.	Annual mean surface air temperature (SAT) records for three sites	23
1-6.	Model sensitivity	28
2-1.	Site location of the paired meteorological stations at Soapgrass Mountain in the Cascade Mountains, Oregon, USA	42
2-2.	Photographs of the Soapgrass Mountain site	43
2-3.	Meteorological and subsurface data observed at the Soapgrass Mountain Open Area (SMOA)	46
2-4.	Soil moisture and precipitation	49
2-5.	Meteorological and subsurface data observed at the Soapgrass Mountain Mature Forest (SMMF)	51
2-6.	Precipitation, temperatures, and soil moisture at the Soapgrass Mountain Mature Forest associate with a heavy precipitation event in 2003	55
2-7.	Differences of meteorological and subsurface data between the Soapgrass Mountain Open Area and Mature Forest	56
2-8.	Snow depth and temperature change for SMOA and SMMF in 2002	59

2-9. Snow depth comparisons 64

2-10. Soil moisture from observations and modeling results for SMOA.....65

2-11. Soil moisture from observations and modeling results for SMMF.....66

2-12. Subsurface temperature from observations and modeling for SMOA.....67

2-13. Subsurface temperature from observations and modeling for SMMF.....68

3-1. Map of northwestern Utah, USA, showing the Emigrant Pass Observatory.....81

3-2. The Emigrant Pass geothermal climate change observatory EPO.....83

3-3. Diffusion of a sinusoidal annual surface temperature wave into the subsurface...85

3-4. Basic aspects of using borehole temperatures to understand surface temperature change.....87

3-5. Meteorological variables and ground temperatures at EPO for the year 2007.....91

3-6. Air and ground temperatures at EPO over the course of one week in October of 2009.....93

PREFACE

This dissertation comprises three individual journal articles written while at the University of Utah and are presented here as separate chapters. The chapters each deal with the relationship between ground temperatures, surface meteorological parameters, such as surface air temperature, solar radiation, precipitation, and snow cover, and different vegetation cover.

The primary question that has focused this research is "Do ground temperatures track air temperatures on both short and long time scales?" Additionally, "What is the effect of changing land cover on ground temperatures?" These questions have an impact on the interpretation of temperature-depth profiles as a tool to determine recent climate change history. If we are to use ground temperatures as a paleoclimate indicator, the connection between air and ground temperatures must be understood well. Two points that are addressed in this dissertation are, first, the tracking of air temperatures by ground temperatures on decadal time scales in boreholes and second, the impact that changing vegetation cover has on air-ground temperature tracking.

Chapter 1 presents an investigation of repeat temperature-depth logs from boreholes in northwestern Utah. It was published in volume 115 of the *Journal of Geophysical Research – Solid Earth* under the title "Repeat temperature measurements in boreholes from northwestern Utah link ground and air temperature changes at the decadal

time scale," by M. G. Davis, D. S. Chapman, and R. N. Harris in May of 2010. This article is reproduced here with permission from the American Geophysical Union. Chapter 2 is being prepared for submission to *Agricultural and Forest Meteorology* under the title "Subsurface thermal and hydrological changes between a forested and a clear-cut site in the Oregon Cascades," by M. G. Davis, D. S. Chapman, R. N. Harris, and R. S. Waschmann. This chapter details the investigation of two meteorological stations in the Cascade Mountains of Oregon under differing conditions of land cover. The third and final chapter presents efforts of science outreach through dissemination of observational data and lesson plans at the Emigrant Pass Observatory website. This final article has been published in the *Journal of Geoscience Education* in August of 2012 under the title "A web-based resource for investigating environmental change: the Emigrant Pass Observatory" by M. G. Davis and D. S. Chapman. It is reproduced here with permission from the National Association of Geoscience Teachers.

I wish to thank the many friends and colleagues who have contributed to my work at the University of Utah. In particular, my doctoral committee, Dave Chapman, Rob Harris, John Bowman, Kip Solomon, and Dave Bowling, have given me support and encouragement throughout this process. My advisor, David Chapman, is owed distinct thanks for getting me started on this journey so long ago when he convinced an undergraduate interested in volcanoes to do a senior thesis on thermal conductivity anisotropy. Little did I know that it would lead me back to Utah to study ground temperatures and climate change. In addition, much appreciation and thanks are due to the many student members of The Friends of Lord Kelvin (FoLK) group during my time at the University, including Paul Gettings, Derrick Hasterok, Christian Hardwick,

Kristine Nielson, Sukanta Roy, Imam Raharjo, Melissa Masbruch, Mason Edwards, and Bryce Johnson. Paul Gettings is owed especial thanks for so many trips to measure ground temperatures or fix sensors, often in adverse weather.

I would also like to thank my family for their support of my academic pursuits. My children, Marisa, Thomas, Elizabeth, and Caitlin have always thought it was cool that dad was in school along with them. They have been an inspiration to me, and reminded me that all of us have an innate scientific curiosity. Finally and above all, this work would not have been possible without my loving wife, Tammy. Her love, patience, support, and sacrifice have not gone unnoticed. I remain now and eternally in her debt.

CHAPTER 1

REPEAT TEMPERATURE MEASUREMENTS IN BOREHOLES FROM NORTHWESTERN UTAH LINK GROUND AND AIR TEMPERATURE CHANGES AT THE DECADAL TIME SCALE

Abstract

Borehole temperature profiles provide a record of ground surface temperature (GST) change at the decadal to centennial time scale. GST histories reconstructed from boreholes are particularly useful in climate reconstruction if changes in GST and surface air temperature (SAT) are effectively coupled at decadal and longer time periods and it can be shown that borehole temperatures respond faithfully to surface temperature changes. We test these assumptions using three boreholes in northwestern Utah that have been repeatedly logged for temperature over a time span of 29 years. We report thirteen temperature-depth logs at the Emigrant Pass Observatory (EPO) borehole GC-1, eight at borehole SI-1, and five at borehole DM-1, acquired between the years 1978 and 2007. Systematic subsurface temperature changes of up to 0.6 °C are observed over this time span in the upper sections of the boreholes; below approximately 100 m any temperature transients are within observational noise. We difference the temperature logs to highlight

subsurface transients and remove any ambiguity resulting from steady-state source of curvature. Synthetic temperature profiles computed from SAT data at nearby meteorological stations reproduce both the amplitude and pattern of the transient temperature observations, fitting the observations to within 0.03 °C or better. This observational confirmation of the strong coupling between surface temperature change and borehole temperature transients lends further support to the use of borehole temperatures to complement SAT and multiproxy reconstructions of climate change.

Introduction

Borehole temperature-depth profiles contain important information about the Earth's changing surface temperature [*Lachenbruch and Marshall*, 1986; *Pollack and Chapman*, 1993; *Pollack and Huang*, 2000; *Beltrami*, 2002; *Harris and Chapman*, 2005]. For one-dimensional, conductive heat transfer, a surface temperature variation in time,

$$T(z=0,t)=F(t), \tag{1-1}$$

creates transient curvature in the subsurface temperature profile, with the subsurface temperature response being governed by the diffusion equation,

$$\frac{\partial T(z,t)}{\partial t}=\alpha\frac{\partial^2 T(z,t)}{\partial z^2}, \tag{1-2}$$

where T is temperature, z is depth, t is time, and α is thermal diffusivity. The diffusion of the surface temperature variation into the subsurface is scaled by thermal diffusivity. A

surface temperature change at time zero is largely captured within a depth called the thermal length, l,

$$l = \sqrt{4\alpha t}\ , \qquad (1\text{-}3)$$

at a subsequent time t. Because the thermal diffusivity of rocks is about 1 x 10^{-6} m^2 s^{-1}, the majority of the past 100 years of surface temperature change is stored within the upper 113 m of the Earth; the majority of the last 1000 years of surface temperature change is captured in the uppermost 350 m. Careful analysis of curvature in the upper few hundred meters of a temperature-depth profile, therefore, can be used to reconstruct surface temperature change over the past millennium [e.g., *Huang et al.*, 2000; *Harris and Chapman*, 2001; *Pollack and Smerdon*, 2004].

Equation 2 posits that for a homogeneous half space, the rate of change of temperature at any depth is proportional to the transient curvature in the temperature-depth profile at that depth. Because the Earth is not a homogeneous half space, phenomena and processes other than a changing surface temperature can also cause curvature in temperature-depth profiles. Steady-state source of curvature include: subsurface thermal conductivity variation, radioactive heat production, refraction due to topography, and by differential solar insolation due to variations in slope and azimuth. Transient source of curvature include: changes in GST due to surface air temperature (SAT), spatial changes in surface temperature around the borehole caused by temporal variations in albedo, nonisothermal groundwater flow [e.g., *Beck*, 1982; *Chisholm and Chapman*, 1992; *Lewis and Wang*, 1992; *Harris and Chapman*, 1995], precipitation

[*Bartlett et al.*, 2004], and other microclimatic effects. *Chisholm and Chapman* [1992] and *Harris and Chapman* [1995] explore the magnitude of many of these effects quantitatively. While most studies of climate change inferred from borehole temperature profiles attempt to select sites that minimize these nonclimatic sources of borehole temperature profile curvature, it is often difficult to partition curvature between steady-state and transient sources of curvature. Much of the ambiguity in interpreting borehole temperature-depth curvature can be removed by measuring the transient effect directly.

Direct observation of the transient temperature field in a borehole temperature profile has a second important consequence. If there is a meteorological station at the borehole site, or reasonably close, then the linkage between changes in the surface air temperature (SAT) with time and changes in the subsurface temperature-depth profile can also be evaluated. How strongly coupled are ground surface temperature (GST) histories to changes in SAT? Such a test is the basis of using borehole temperatures to reconstruct climate change and for comparing the results of borehole studies with SAT changes and also proxy temperature changes over longer periods.

At the annual to decadal scale, coupling between SAT and GST has been investigated through comparisons between meteorological data and shallow soil thermistors [e.g., *Putnam and Chapman*, 1996; *Smerdon et al.*, 2004, 2006; *Bartlett et al.*, 2006; *Stieglitz and Smerdon*, 2007]. Related studies include model simulations which parameterize relevant processes at the ground surface to simulate interactions between the atmosphere and subsurface [e.g., *Gonzalez-Rouco et al.*, 2003, 2006, 2009], comparisons between atmospheric models and observed borehole temperature profiles [*Beltrami et al.*, 2006; *Stevens et al.*, 2008], and comparisons between hemispheric

averages of SAT and borehole temperature data [*Harris and Chapman*, 2005; *Harris*, 2007].

In spite of the importance of direct observation of borehole temperature transients, the slow rate of temperature change combined with the difficulty of maintaining access to sites over more than decades has resulted in only a few studies of repeat borehole temperature measurements [*Chapman and Harris*, 1993; *Majorowicz and Safanda*, 2005; *Safanda et al.*, 2007; *Kooi*, 2008]. *Chapman and Harris* [1993] used the differences between repeat borehole temperature logs from northwest Utah to show that subsurface temperature transient can be determined and steady-state sources of curvature can be eliminated. More recent studies by *Majorowicz and Safanda* [2005], *Safanda et al.* [2007], and *Kooi* [2008] echo the findings of *Chapman and Harris* [1993], as well as show that multiple temperature-depth logs from individual boreholes can decidedly resolve uncertainty between SAT and GST coupling.

In this study, we report direct observations of transient temperatures in three boreholes from northwest Utah. Observations include repeated temperature logs collected over a 29-year time span. At one borehole, site GC-1, we use a collocated meteorological station (Emigrant Pass Observatory – EPO), established in 1993, to investigate fine-scale coupling between air and ground temperatures. We first isolate the transient temperature field in each borehole and then quantitatively compare variations in these temperature logs with variations in SAT from nearby meteorological stations. This study extends the time span of observations and expands the number of sites used in the earlier work of *Chapman and Harris* [1993].

Borehole Temperature-Depth Profiles

Boreholes at Grouse Creek (GC-1), Silver Island (SI-1), and Desert Mountain (DM-1) (Figure 1-1) were drilled in 1978 as part of a heat flow investigation of the northern Basin and Range tectonic province in the western U.S [*Chapman et al.*, 1978]. These boreholes were specifically located in granitic plutons with subdued terrain to minimize disturbances due to rock heterogeneity and topography and to minimize possible disturbances from groundwater flow. Each borehole was drilled to a depth of 152 meters and cased with 64 mm inner diameter PVC pipe. The annulus was back-filled with a slurry of drill cuttings. The bottoms of the casings were capped and the pipes were filled with water to stabilize the measuring environment and facilitate temperature logging.

Borehole GC-1 is located in northwestern Utah at the southern edge of the Grouse Creek Mountains (Figure 1-1). The environment surrounding GC-1 is classified as desert. The jet stream brings storms from the Pacific Northwest to northern Utah, and much of the roughly 30 cm annual precipitation at the site comes in the form of snow [*Bartlett et al.*, 2006]. Borehole SI-1 is located on the western flank of the Silver Island Mountains on the west side of the Great Salt Lake. This range is surrounded by playa, salt, and mud flats from remnants of higher stands of the lake. Precipitation is low in the area as evidenced by the desert conditions and salt flats. Borehole DM-1 is located near the eastern edge of the Great Basin. Grasses and occasional sagebrush on the generally flat and low-lying basin dominate the semi-arid desert environment, giving it a more steppe-like setting.

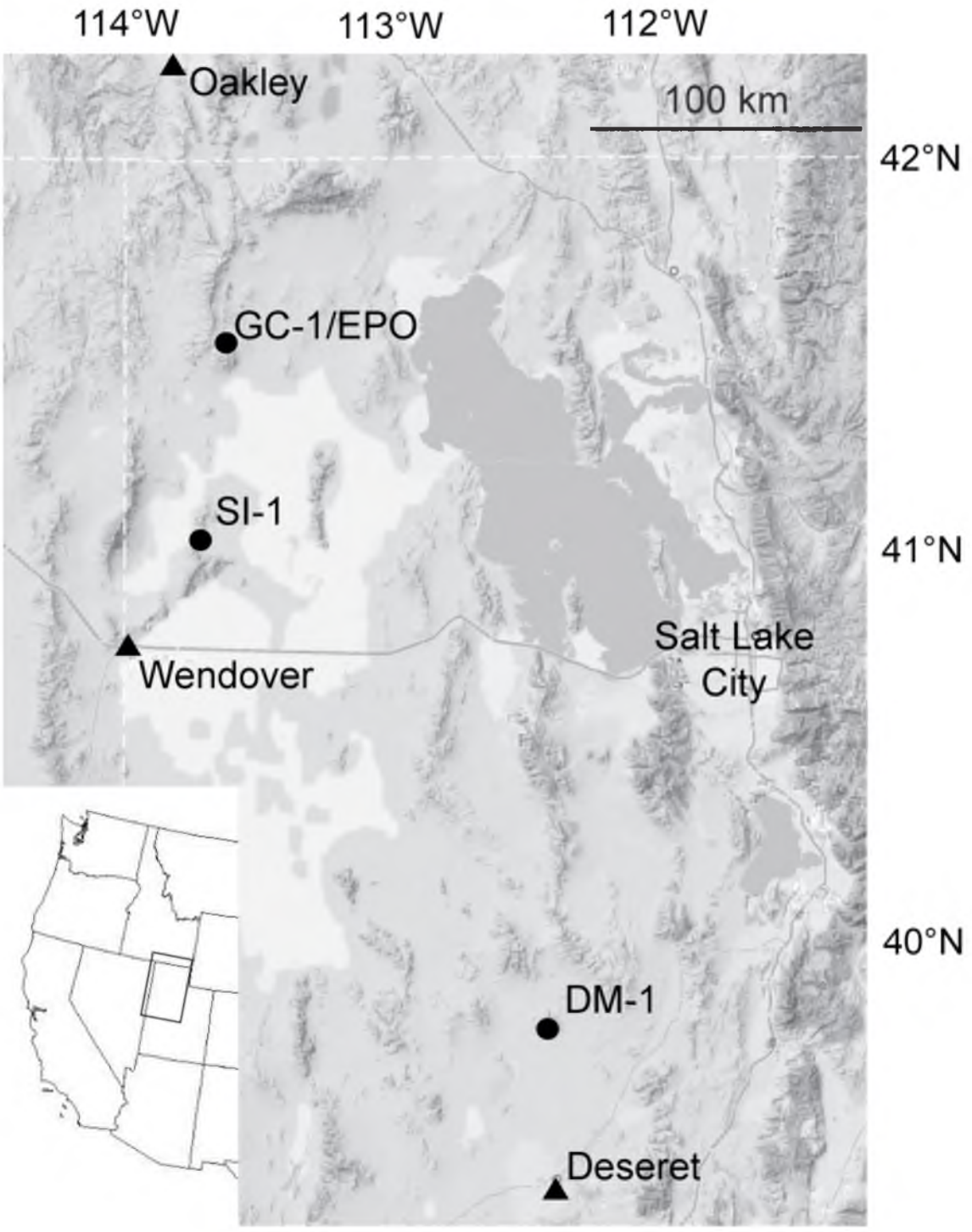

Figure 1-1. Location map of northwestern Utah, USA, showing borehole sites (circles) and meteorological stations (triangles) used for comparisons between ground and air temperatures. Meteorological stations are from the US Historical Climatology Network [*Menne et al.*, 2009].

Temperature-depth profiles from these boreholes were originally measured in 1978 at a logging interval of 5 m (temperature-depth data are provided in the auxiliary material). Thermal conductivities (Table 1-1) were made on rock chips returned to the surface during drilling and are relatively uniform with depth [*Chapman et al.*, 1978]. A changing focus in geothermal studies from heat flow to climate change caused us to relog the boreholes in 1990, decreasing the depth interval of temperature measurements from 5 to 1 m to improve resolution of any possible climatic signal [*Chisholm and Chapman*, 1992]. Starting in 1992, multiple logs within the same field session were measured and averaged (Table 1-2) with the aim of reducing noise from random temperature fluctuations within the borehole [*Chapman and Harris*, 1993; *Harris and Chapman*, 2007]. A waiting time of about 12 hours between logs ensured that the thermal conditions in the borehole had equilibrated from disturbances caused by the previous log.

Temperature-depth profiles from the three boreholes taken over a span of 29 years are shown in Figure 1-2. To account for instrument (thermistor, resistance meter) drift over the nearly three decades and small uncertainties in depth, the temperature data for each log are shifted by a small amount so that bottom hole temperatures are constant for all logs at each borehole (Table 1-2). Each temperature shift is typically less than a few 10s of milliKelvin and improves the consistency of the lower portion of each temperature profile. The lower portion of each temperature log exhibits a constant thermal gradient, consistent with the observed uniform thermal conductivity and constant heat flow. We define a background thermal regime and surface temperature intercept at each site in terms of a linear fit to data below a depth of 100 m (Table 1-1). These parameters are based on the entire set of temperature logs for each borehole. The

Table 1-1. Geothermal information for borehole sites.

Borehole	Latitude	Longitude	Elevation (m)	Γ (°C/km)	T_o (°C)	K ($W\ m^{-1}\ K^{-1}$)	Heat Flow ($mW\ m^{-2}$)
GC-1	41°32'	113°42'	1756	31.03	10.65	3.14	97
SI-1	41°02'	113°47'	1332	40.54	13.93	2.28	92
DM-1	39°44'	112°36'	1524	31.64	14.22	3.01	95

Γ is the average thermal gradient and T_o is the average surface temperature intercept based on linear fits to the data below 100 m for all temperature logs. K is the thermal conductivity.

Table 1-2. Logging years and numbers of borehole logs used in analysis.

Borehole	Year	Number of Logs	Γ °C/km	T_o °C	ΔT_b °C	Notes
GC-1	1978	1	31.19	10.63	0.105	5m spacing
	1990	1	31.08	10.65	0.012	1m spacing
	1992	3	31.24	10.62	0.007	
	1993	4	31.19	10.63	0.010	
	1994	3	31.04	10.65	-0.020	Small diameter pipe
	1995	3	30.88	10.68	0.027	
	1996	3	31.03	10.66	-0.026	
	1998	1	30.54	10.73	0.042	
	2000	3	31.03	10.66	-0.028	
	2002	3	31.05	10.65	-0.031	
	2004	2	31.04	10.65	-0.030	
	2005	1	31.06	10.65	-0.029	
	2007	2	31.09	10.65	-0.039	
	Ave		31.03	10.65		
SI-1	1978	1	41.92	13.72	0.088	5m spacing
	1990	1	40.55	13.93	0.004	1m spacing
	1992	3	40.44	13.94	-0.007	
	1994	4	40.26	13.95	-0.014	
	1995	3	40.44	13.94	-0.011	
	1996	3	40.32	13.96	-0.023	
	1997	3	40.30	13.96	-0.012	
	2007	2	40.11	13.99	-0.026	
	Ave		40.54	13.93		
DM-1	1978	1	31.69	14.20	0.125	5m spacing
	1990	1	31.81	14.20	-0.026	1m spacing

Table 1-2. continued.

1992	3	31.69	14.23	-0.015
1997	3	31.63	14.24	-0.023
2007	1	31.40	14.26	-0.061
Ave		31.64	14.22	

Γ is the thermal gradient and T_o is the surface temperature intercept based on linear fits to the data below 100 m. ΔT_b is the shift applied to the temperature logs assuming the bottom hole temperature is constant. The average values at the bottom of each log set are used to reduce the data after applying the temperature shift.

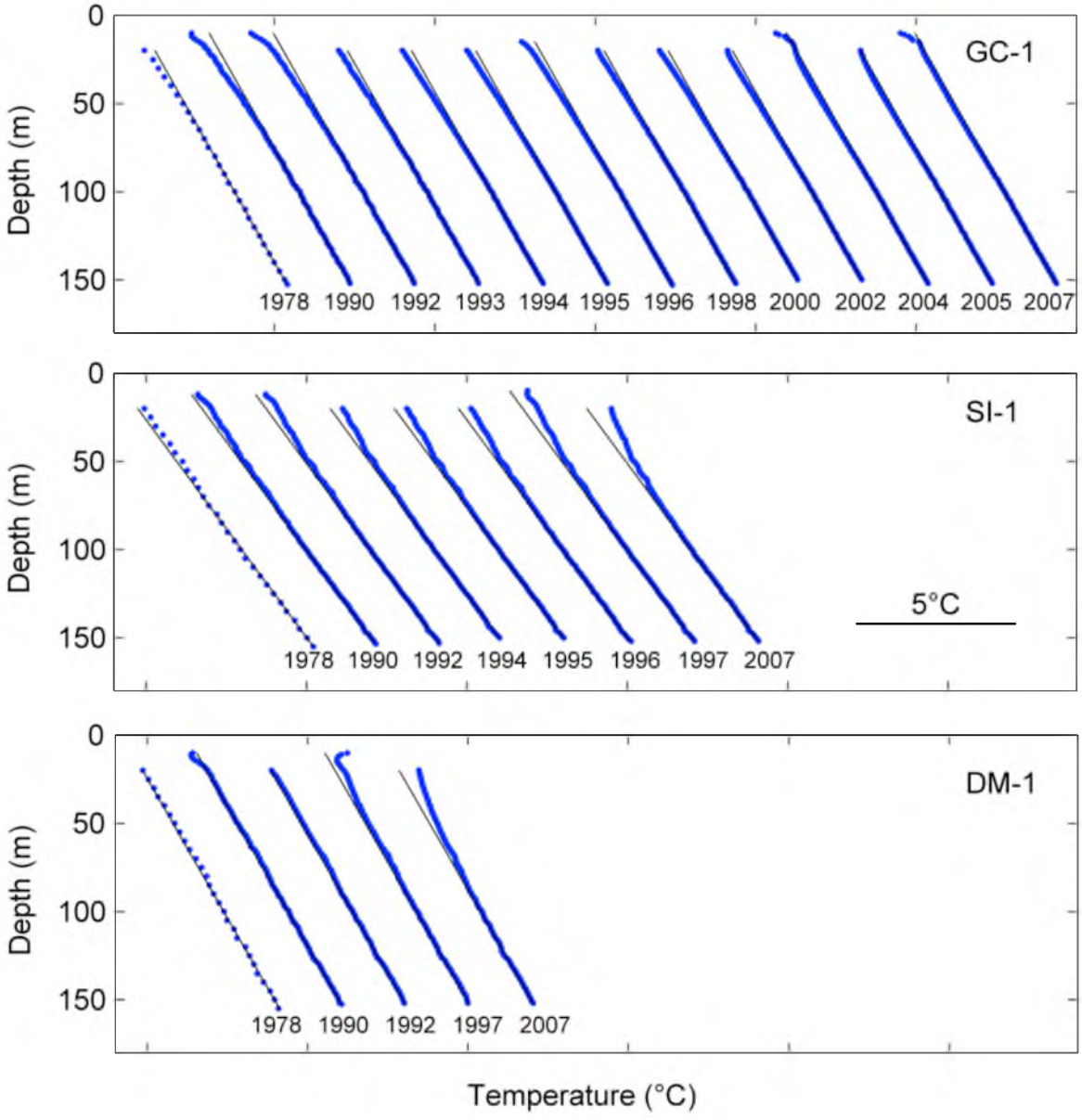

Figure 1-2. Temperature-depth profiles collected between 1978 and 2007 from boreholes GC-1 (top), SI-1 (middle), and DM-1 (bottom). Plots are offset to avoid overlap. Temperature-depth profiles are averaged when multiple logs were collected during the same field campaign (Table 2). Also shown is the background thermal gradient (solid lines) determined from the data below 100 m.

repeated temperature logs cover a period of 29 years that corresponds to a thermal length of approximately 60 m. The choice of 100 m as the start of the fitting depth represents a trade-off between starting below recent climatic effects and using as much data as possible to obtain a robust gradient fit [*Chisholm and Chapman*, 1992]. The average surface temperature intercepts (Table 1-1) are appropriate for this geographic latitude, elevation, and climatic setting. Heat flow at the three sites computed as the product of the thermal gradient and thermal conductivity is 97, 96, and 95 mW m^{-2}, appropriate for the Basin and Range tectonic setting [*Chapman et al.*, 1978]. The observation that the thermal gradient and surface temperature intercept are consistent with the tectonic and geographic setting adds confidence that heat transfer at these sites is dominantly conductive.

The upper portion of each borehole (< 100 m) shows systematic departures from the background thermal regime and these departures change with time between 1978 and 2007. To highlight these departures, we compute reduced temperature profiles for each log by removing the average thermal gradient and surface temperature intercept. By using the average thermal gradient and surface temperature intercept to compute reduced temperatures, each log is reduced to the same datum. Results are shown in Figure 1-3 and the reducing parameters are tabulated in Table 1-1. The reduced temperatures plotted on an expanded scale display coherent patterns, as well as instrumental and geologic noise.

Several features of the reduced temperature logs merit discussion. In general, the bottom portion of each reduced temperature profile is relatively constant with near zero reduced temperatures indicating that the fitting depth starting at 100 m is appropriate.

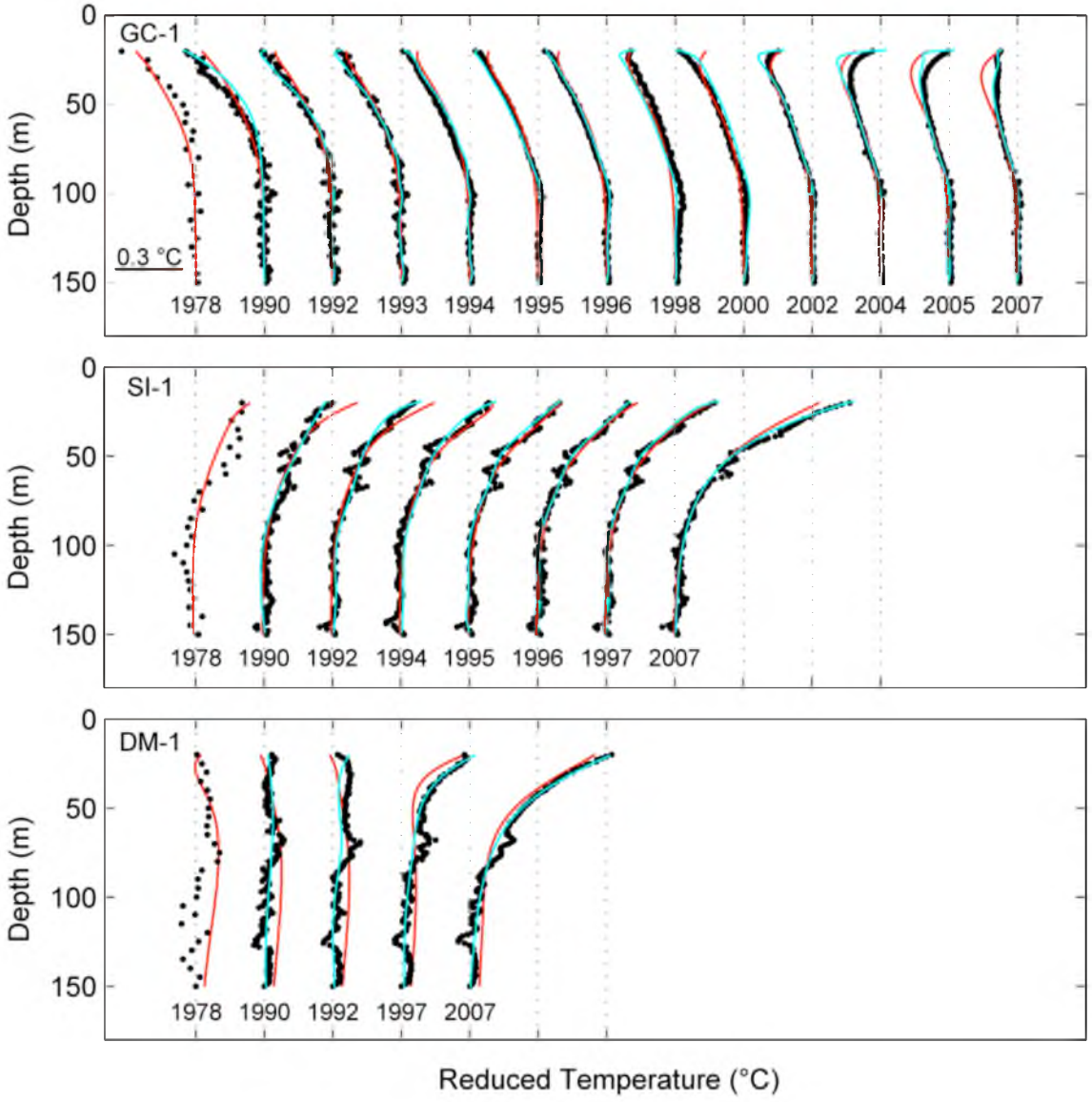

Figure 1-3. Reduced temperatures (dots) for boreholes GC-1 (top), SI-1 (middle), and DM-1 (bottom). Cyan lines show the previous log forward continued in time assuming a linear change in surface temperature. Red lines show synthetic transient temperature profile constructed from the associated meteorological station data: EPO for GC-1, Wendover for SI-1, and Deseret for DM-1.

Close inspection of the bottom third of reduced temperature profiles at GC-1 shows a conspicuous fine structure with an amplitude of approximately 0.03 °C and a characteristic length of 4 m. This scatter is also evident in the 1978 log, but at reduced resolution because of the 5 m measurement spacing. Similar but somewhat larger amplitude fine structure is observed in the reduced temperature logs for both SI-1 and DM-1. *Chisholm and Chapman* [1992] and *Chapman and Harris* [1993] postulated that the fine structure was caused by convective instabilities in the borehole, thermal conductivity changes, groundwater flow in either the borehole or the granite, or small depth offsets. Starting in 1992, multiple temperature logs at each borehole were collected during each field campaign to understand this structure better. If the variations were random in space or time, averaging and stacking logs should diminish these oscillations. Instead, the small temperature irregularities remained a persistent pattern demonstrating that they are stationary in time and space.

In 1993, after measuring the temperature logs at GC-1, we installed a small diameter pipe (2.54 cm ID) inside the casing and attached convective baffles to the outside of the inner pipe. The 1994 and subsequent logs show that the oscillations are greatly reduced, suggesting that the oscillations were the result of convection in the borehole. *Harris and Chapman* [2007] summarized several lines of evidence to suggest that the fluctuations were the result of stationary convection, and may be due to heterogeneities in the borehole diameter or less likely thermal properties of the rock that establishes any convection in space.

The second feature meriting discussion, and more salient to this paper, is the uppermost portion of each reduced temperature profile. At GC-1, reduced temperature

values are negative, indicating surface cooling relative to the background thermal regime prior to 1978. With time, the magnitudes of the reduced temperature become less negative, consistent with recent warming. In contrast to GC-1, reduced temperature profiles at SI-1 and DM-1 are positive in the upper reaches of the borehole and show similar changes over the 29-year time span between 1978 and 2007. At 20 m, the reduced temperature at both sites increases approximately 0.6° C during this period, from 0.15° C to 0.75° C in the case of SI-1 and from 0° C to 0.65° C at DM-1. During this same period, the anomaly shifts downward by approximately 20 m from ~ 70 to ~ 90 m. The pattern of reduced temperatures at all three boreholes is consistent with ongoing and persistent surface warming.

To test if these patterns of reduced temperature are quantitatively consistent with surface temperature variations, we forward continue each log into the following log (cyan line, Figure 1-3). In this procedure, we use a Laplace transform on the current log and, in an iterative procedure, find the linear trend that produces the minimum misfit when this log is forward continued and compared to the following log [*Harris and Chapman*, 2005]. The Laplace transform uses the first log as the initial condition so that a reference temperature does not need to be used. In this manner, the 1978 log is forward continued into the 1990 log, the 1990 log is forward continued into the 1992 log, and so on. This forward continuation modifies the temperature observations according to the diffusion equation in two ways. High wavenumber variations are attenuated and because each linear change is positive, anomalous temperatures have greater magnitude at greater depths relative to the original profile. The assumption of a linear change in surface temperature is the most conservative scenario that incorporates a changing surface

condition. In general, the fits at long wavenumbers are very good. It is interesting to note that the high wavenumber oscillations in the lower part of the reduced temperature profiles are effectively diffused away over periods of 1 and 2 years, for example, as shown by the 1990, 1992, and 1993 logs at GC-1 and their forward continuation, or the high wavenumber variations between approximately 40 and 60 m in borehole SI-1. Unfortunately, because in most cases logging starts at a depth of 20 m, below the penetration of the high amplitude annual wave, we do not have great sensitivity to the magnitudes of the linear trends and a range of trends fit the data equally well. However, all linear trends indicate ongoing surface warming. To explore sensitivity over the full time period of repeat logs, we forward continued the initial logs into the most recent logs to estimate the linear change in surface temperature. The amplitude of the temperature change computed from best-fit linear trends between 1978 and 2007 are 0.9, 0.7 and 0.7° C, at GC-1, SI-1 and DM-1, respectively (Table 1-3). The amplitude of each linear trend is the same within uncertainties consistent with their geographic settings and proximity. Sensitivity is improved and root mean square (RMS) misfits are 0.01, 0.03, and 0.03° C for boreholes GC-1, SI-1, and DM-1, respectively. The low RMS misfits suggests that the departures from the background thermal regime can be understood in terms of a changing surface temperature condition. The negative reduced temperatures at GC-1 are puzzling (Figure 1-3), but this analysis indicates that over the period for which we have repeated temperature logs, each borehole site shows the same magnitude of warming. The difference in the GC-1 repeat temperature profiles relative to SI-1 and DM-1 is the initially cool state.

Table 1-3. Amplitude of temperature changes between 1978 and 2007.

Borehole	Amplitude of Linear Trend from temperature-depth profiles[1] °C	Amplitude of Linear Trend from SAT data[2] °C
GC-1	0.9±0.2	1.1±0.1
SI-1	0.7±0.3	0.7±0.1
DM-1	0.7±0.3	1.2±0.1

[1]Amplitude of linear trend that minimizes the misfit when the 1978 temperature profile is forward continued into the 2007 temperature profiles. See text for details.
[2]Amplitude of best fitting trend to SAT data between 1978 and 2007.
Uncertainties are 95% confidence limits.

To isolate subsurface temperature variability between 1978 and 2007 and to remove curvature due to steady state processes, we difference the repeated temperature profiles. Figure 1-4 shows differences between temperature logs for each site relative to the original 1978 log. At GC-1, the temperature difference plot for 1990 shows coherent but small negative temperatures between 25 and 70 m that are a maximum at approximately 40 m depth. While this anomaly is small, it is larger than the small fluctuations below 100 m and therefore likely significant. With time, this anomaly spreads out and attenuates so that by 2007 it is centered at a depth of approximately 70 m. Starting in approximately 2002 temperature differences above 30 m in GC-1 become positive and increase with time so that by 2007 positive reduced temperatures extend to a depth of approximately 50 m.

Residual temperature variability at SI-1 is considerably larger than at GC-1, particularly in the shallow part of the borehole (Figures 1-3 and 1-4). At SI-1 between 1978 and 1990, changes in temperature are small and the fluctuations in the 1990 difference profile may mostly reflect noise (Figure 1-4). At about 50 m depth, a high wavenumber negative anomaly appears both persistent and stationary in time. This is in the region of high amplitude variations in the reduced temperature profiles (Figure 1-3) and is likely due to convection. The sharpness of these anomalies indicates that it is probably not due to climatic variations, and indeed is attenuated in the forward continuation analysis. Small temporal variations in convection may be may be responsible for the persistence of this anomaly. Starting with the 1992 log, shallow temperature differences start to show a coherent trend toward positive values and by 2007 this anomaly extends to about 75 m. This depth extent is consistent with 30 years of

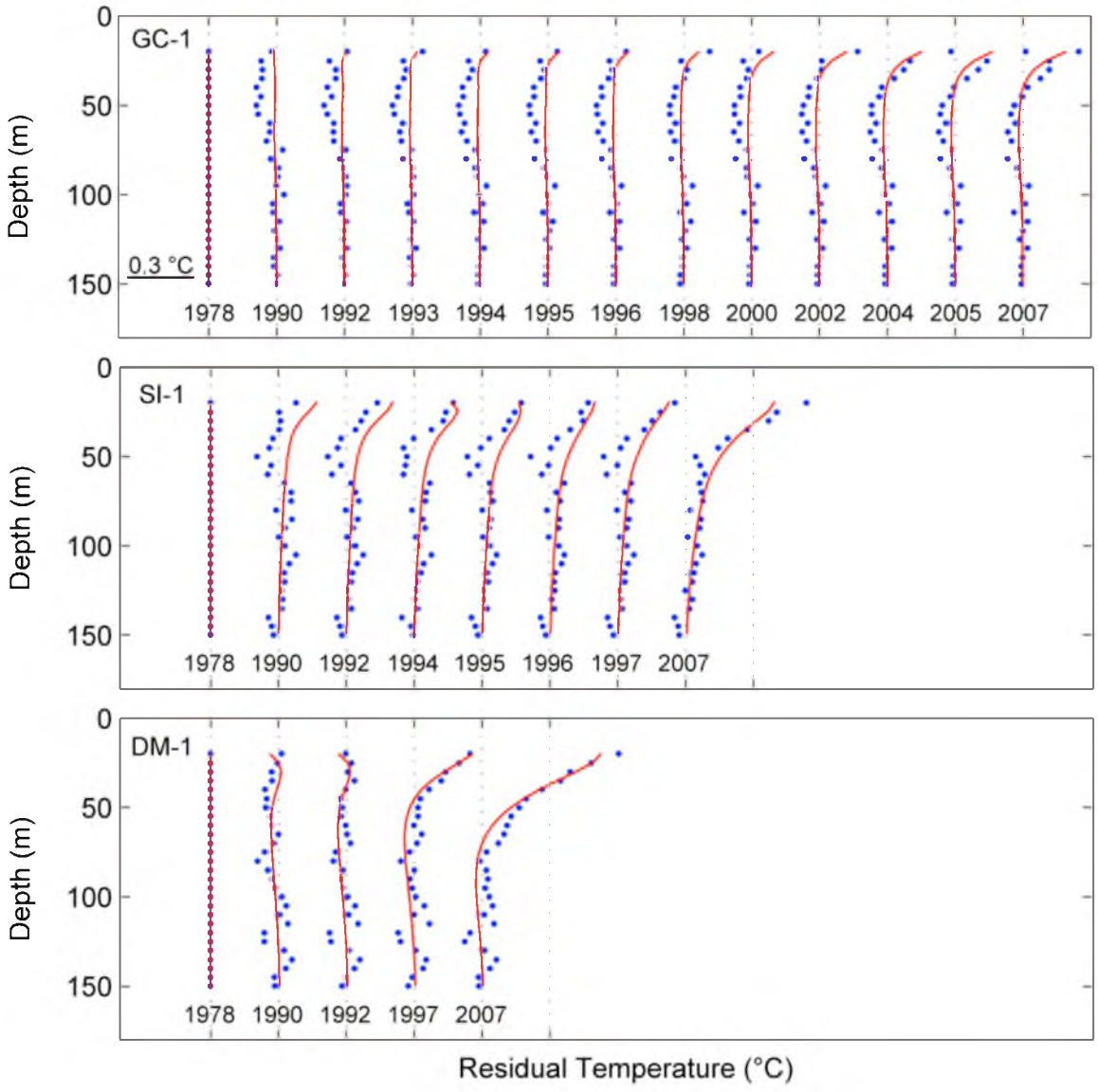

Figure 1-4. Temperature differences (circles) relative to the 1978 log. Model fits (red lines) are computed from the associated surface air temperature records, EPO for GC-1, Wendover for SI-1, and Deseret for DM-1.

warming. At DM-1, trends similar to those observed at SI-1 are present. These differences suggest a stable surface temperature between 1978 and 1992 at DM-1, but by 1997, large temperature differences are present that grow in amplitude and depth through 2007.

Surface Air Temperature Records

To understand these transient borehole temperature variations more quantitatively, we now turn to meteorological data to test if the observed pattern of subsurface temperature changes are consistent with SAT records. Specifically, we use SAT time series as forcing functions at the ground surface and assess how well they can reproduce both the borehole observations of reduced temperature (Figure 1-3) and temperature differences (Figure 1-4).

SAT records reported in this study come from several sources. In the fall of 1993, a meteorological station next to borehole GC-1 (Figure 1-1) was established. Instrumentation and the first annual cycle of data are reported in *Putnam and Chapman* [1996]. *Bartlett et al.* [2006] analyzed the first decade of data and showed that most variability in shallow (0 to 1 m) ground temperatures could be explained by variations in solar insolation during the summer and the presence or absence of snow cover during winter months. For times prior to 1993 and to fill in data gaps, we use SAT data from U.S. Historical Climatology Network (USHCN) stations at Oakley, Idaho, 79 km to the north and Wendover, Nevada, 93 km to the south [*Karl et al.*, 1990; *Menne et al.*, 2009]. Meteorological stations comprising the USHCN have a relatively long temperature time series, a predominantly undisturbed environment around the site, and limited station

relocations. Mean annual departures from these two SATs are conjoined with data from EPO based on weighted averages. Weights are estimated by comparing monthly USHCN data with monthly EPO data over the common period of overlap, 1994 through the present. The best fitting weights are 0.5 for both Oakley and Wendover, likely representing a combination of geographical influences and distance from the EPO site. The composite GC-1 site SAT record uses EPO data where present and the weighted average of data from Oakley and Wendover where EPO data are not present (Figure 1-5).

SAT data used with boreholes SI-1 and DM-1 are from USHCN network stations [*Menne et al.*, 2009]. We compare subsurface temperatures at SI-1 with Wendover, a separation distance of 40 km; subsurface temperatures at DM-1 are compared with Deseret, a separation distance of 50 km. The temperature change amplitude calculated from the linear warming trends between 1978 and 2007 at EPO, Wendover, and Deseret are 1.1, 0.7 and 1.2° C, respectively, and can be directly compared with those obtained from boreholes (Table 1-3). Like the linear trends fit to the reduced temperature logs in the forward continuation analysis, these linear trends are also approximately the same.

Temporal Changes in Subsurface Temperature

For comparison purposes, we produce synthetic reduced temperature profiles for each site by assuming that the SAT time series represents the surface forcing function at each borehole. The SAT series is diffused into the Earth as a sequence of n individual step functions of amplitude ΔT_i and time prior to the borehole temperature log, τ,

$$T_i(z) = (POM - T_1)erfc\left(\frac{z}{\sqrt{4\alpha\tau_1}}\right) + \sum_{i=2}^{n} \Delta T_i erfc\left(\frac{z}{\sqrt{4\alpha\tau_i}}\right), \qquad (1\text{-}4)$$

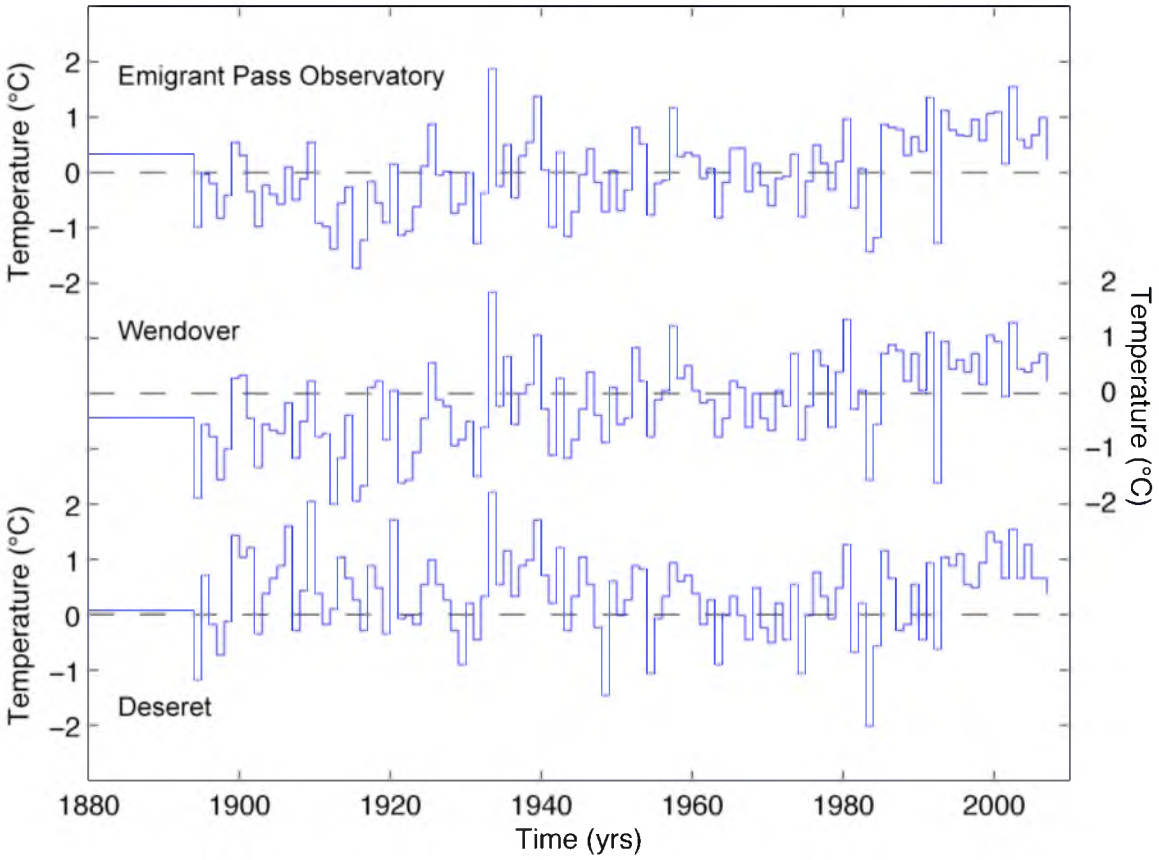

Figure 1-5. Annual mean surface air temperature (SAT) records for three sites. Data for Wendover and Deseret are drawn entirely from the US Historical Climatology Network used in this study. Data for Emigrant Pass Observatory include a weighted average of annual means from Oakley, ID, and Wendover, NV, from 1890 to 1993, and the on-site observatory EPO since 1993. Annual means are relative to the 1961-1990 mean temperature.

where the two unknowns are the pre-observational mean, *POM*, [*Chisholm and Chapman*, 1992], and the thermal diffusivity, α. The complementary error function is denoted by *erfc*. The *POM* is the initial condition corresponding to the long-term mean temperature and represents a weighted average surface temperature prior to the beginning of the meteorological data. In practice, it is determined by minimizing the misfit between the SAT record and the reduced temperature profile [*Harris and Chapman*, 2001]. Just as the reduced temperatures are defined relative to T_o, changes in SAT are defined relative to the *POM*.

Figure 1-3 shows synthetic borehole temperature profiles produced from SAT data for each reduced temperature log. In general, the fits are quite good with synthetic transients fitting both the magnitude and depth extent of reduced temperatures.

The *POM* associated with the GC-1/EPO comparison is greater than the 1961-1990 annual mean (Table 1-4) and this combination produces the negative reduced temperatures observed in the logs. By 1990, annual temperatures largely exceed the *POM*, but positive reduced temperatures are still not observed below 20 m, although there is strong evidence of warming temperatures in the upper portion of GC-1 by the late 1990s, as shown in by the positive hook in reduced temperatures (Figure 1-3). The *POM* associated with the SI-1/Wendover comparison is almost half a degree below the 1961-1990 mean temperature. This relatively low *POM* produces the strong warming observed in the SI-1 model fits. Finally, the *POM* associated with the DM-1/Deseret comparison is close to the 1961-1990 mean temperature and accounts for the relatively small reduced temperatures until about 1997 when the annual means are well above the 1961-1990 mean temperature.

Table 1-4. POM and thermal diffusivity for synthetic temperature calculations.

Borehole	POM °C	α x 10^{-6} m^2 s^{-1}	RMS °C
GC-1	0.33±0.05	0.27±0.06	0.008
SI-1	–0.44±0.03	1.03±0.67	0.008
DM-1	0.08±0.05	1.66±0.67	0.011

POM is the pre-observation mean and α is the thermal diffusivity. Uncertainties are 95% confidence limits. The *POM* is relative to the 1961 – 1990 mean temperature.

It is interesting to note discrepancies between the synthetic and observed transient temperatures. At GC-1, discrepancies are present in the 2004, 2005, and 2007 comparisons (Figure 1-3). Synthetic profiles show a cooling 'bulge' that is associated with the generally low temperatures between approximately 1960 and 1980 at EPO (Figure 1-5). This feature is not very well captured by the reduced temperatures, although the forward diffusion model with linear surface temperature change does reproduce it well (Figure 1-3), as do the temperature differences (Figure 1-4). This discrepancy does not seem to be correlated with either snow or rain events, factors not taken into account with our simple model. It is possible that subtle changes in micrometeorological variables at the site may account for this discrepancy at GC-1. At SI-1 starting in 1990, the shallow portion of the synthetic profile is warmer than the reduced temperature. With time, the reduced temperatures become more positive than the synthetic, suggesting that the ground at SI-1 is warming more quickly than the SAT data at Wendover. At DM-1, the synthetic profile fits the reduced temperature profile general shape extremely well at long wavelengths but does not fit short wavelength fluctuations particularly well. Part of these misfits may be due to steady-state curvature in the reduced temperature profiles not related to surface temperature change.

The temperature difference logs (Figure 1-4) avoid complications from steady-state processes or effects that cause curvature in temperature-depth profiles. We produce synthetic difference profiles from SAT data by computing diffused versions of the forcing function between 1978 and successive logging times in a single step using,

$$T_{res}(z) = \left[(POM - T_1) erfc\left(\frac{z}{\sqrt{4\alpha(\tau 1)_1}} \right) + \sum_{i=2}^{n1} \Delta T_i erfc\left(\frac{z}{\sqrt{4\alpha(\tau 1)_i}} \right) \right]$$
$$- \left[(POM - T_1) erfc\left(\frac{z}{\sqrt{4\alpha(\tau 2)_1}} \right) + \sum_{i=2}^{n2} \Delta T_i erfc\left(\frac{z}{\sqrt{4\alpha(\tau 2)_i}} \right) \right], \quad (1\text{-}5)$$

where the terms in the first bracket refer to the 1978 log and terms in the second bracket refer to the second log. We explicitly show this equation to emphasize that while each temperature difference (ΔT_i) prior to 1978 is the same, the weights change slightly because of the difference in time prior to the respective logs, either $\tau 1$ or $\tau 2$. At GC-1 and SI-1, the modeled differences show a monotonic warming trend consistent with general warming trends in the SAT forcing function relative to the 1961-1990 mean temperatures (Figure 1-4). At Deseret, there is a sharp step in warming at about 1995 and this is manifested in the modeled difference as a strong warming trend. These plots show that in general, ground temperatures at GC-1 and DM-1 between 1978 and 2007 have kept pace with warming at their associated surface air temperature sites, while ground temperatures at SI-1 appear to be warming more quickly than those at Wendover.

Finally, we investigate the sensitivity of our solutions to the two free parameters *POM* and α. Figure 1-6 panels a-c show the RMS misfit comparisons between reduced temperature (Figure 1-3) at each borehole, GC-1, SI-1, and DM-1 and the synthetic profile computed from its associated SAT record; Figure 1-6 panels d-f show results for the temperature difference plots (Figure 1-4) and the synthetic profile differences. In all cases, the models fit the data within an RMS value of 0.02 °C. In general, the fits are most sensitive to the *POM* and relatively insensitive to thermal diffusivity (Table 1-4).

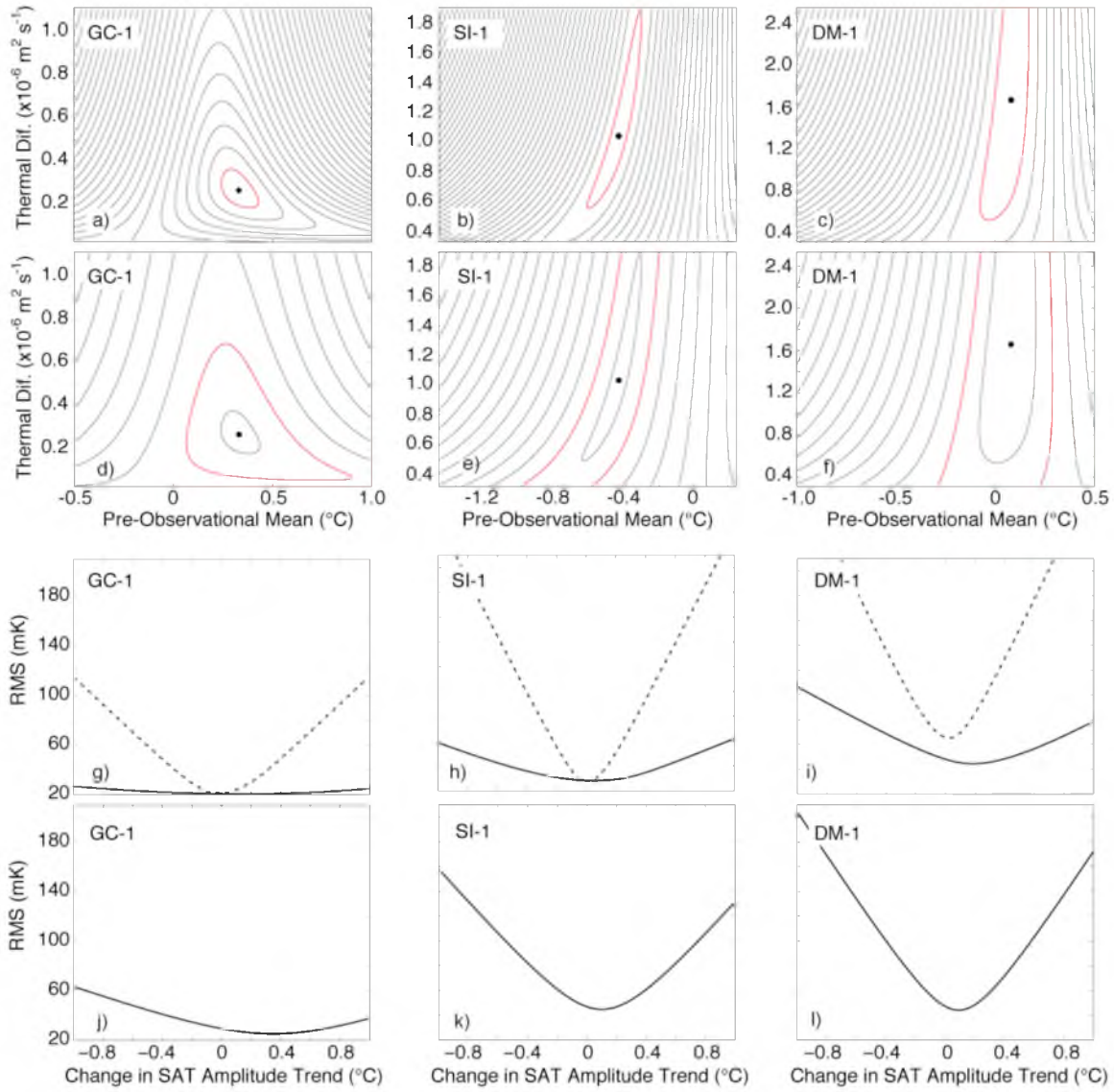

Figure 1-6. Model sensitivity. Panels a-c show RMS misfits between reduced temperature profiles and synthetic temperature profiles calculated from SAT data using Equation 2; panels d-f show RMS misfits between temperature difference profiles and synthetic differences calculated from SAT data using Equation 3. The contour interval is 0.04° C and the inner contour is 0.02 in all six panels. The red contour indicates the 95% confidence interval. Panels g-i show the sensitivity of the model fit between the reduced temperatures and the SAT data to the trend of the SAT data over the entire time series (dashed line) and between 1978 and 2007 (solid line). Panels j-l show the sensitivity of the model fit between the difference profiles and the SAT data to the trend of the SAT data between 1978 and 2007.

The optimum thermal diffusivity at SI-1 and DM-1 are close to 1 x 10^{-6} m^2 s^{-1}, a default value in many geothermal studies of climate change. At GC-1, the best fitting thermal diffusivity is 0.3 x 10^{-6} m^2 s^{-1}. *Bartlett et al.* [2006] estimated the thermal diffusivity at GC-1 based on daily temperature series at depth of 0.1 and 1.0 m between 1993 and 2004. They found that the best fitting daily mean thermal diffusivity had a range of 0.78—0.96 x 10^{-6} m^2 s^{-1} with a mean value of 0.88 x 10^{-6} m^2 s^{-1}. Our lower value may be due to a slight depth dependence of thermal diffusivity or surface processes not accounted for in the simple diffusion model [*Pollack et al.*, 2005]. Further, the increased sensitivity of the thermal diffusivity at GC-1 is likely due to the intermediate wavenumber hook in the shallow subsurface starting about 2002. This added structure increases the sensitivity of the model to the thermal diffusivity.

We show the sensitivity of the reduced temperature profiles to the linear trend in the SAT data by varying the trend of the SAT data over the entire period (Figure 1-6 g-i). The RMS misfit diagrams indicate 1) that the minimum misfit corresponds to the true SAT amplitude at the 95% confidence level (Table 1-5), and 2) good sensitivity to the longest wavelength trend in the SAT series. Both of these observations are consistent with good coupling between air and ground temperatures. The solid lines in Figure 1-6 g-i show the sensitivity of the SAT time series to its linear trend over the 29-year period for which we have repeated temperature profiles. Using a limited SAT period significantly decreases the sensitivity of the SAT record to the reduced temperature profiles.

Differencing the synthetic transients generated with the SAT records (Equation 1-5) decreases the sensitivity to the *POM* and thermal diffusivity (Figure 1-6 d-f) and

Table 1-5. Amplitude of the best-fitting SAT trend.

Borehole	*Reduced Temperature + Entire SAT* °C	*Reduced Temperature + 1978-2007 SAT* °C	*Temperature Differences + 1978-2007 SAT* °C
GC-1	-0.03±0.14	-0.01±0.87	0.35±0.39
SI-1	-0.02±0.08	0.05±0.31	0.10±0.16
DM-1	0.04±0.09	0.19±0.24	0.09±0.12

Values are reported relative to century-long trends such that 0° C is equal to the true trend in the SAT series. Uncertainties are 95% confidence limits.

increases the sensitivity to the SAT forcing function (Figure 1-6 j-l) relative to the reduced temperature (solid lines, Figure 1-6 g-i). In this case, we are comparing SAT trends between 1978 and 2007 to temperature differences logged between 1978 and 2007. For our set of repeated logs, this time interval is the one in which we have greatest sensitivity. For the 1978-2007 time period, the minimum RMS misfits associated with the differenced logs (Figure 1-6 j-l) are slightly larger than for the reduced temperature profiles, but this should not be surprising since these misfits are based on differences. These panels show good sensitivity to the trend during this time interval. In general, the change in best fitting SAT trends are somewhat greater than 0° C at the 95% confidence level, suggesting that the differenced profiles indicate slightly greater warming than the SAT records over this time period (Table 1-5).

Discussion

Repeated temperature logs in northwestern Utah demonstrate significant ground warming over a 29-year time period. The three borehole sites show similar warming trends over the 29-year time period, as do the SAT data. Linear warming trends between the boreholes and the meteorological sites are in good agreement (Table 1-3) and qualitatively suggest coupling. The advantage of repeated temperature logs is the ability to isolate temperature transients within the borehole temperature logs that removes curvature due to steady state processes. A second advantage is increasing sensitivity to SAT records in model fits that provides a more stringent test of ground and air temperature coupling by decreasing sensitivity to the free parameters, the *POM* and thermal diffusivity.

While model fits between air and ground temperatures are not perfect, they are quite good given the: 1) distances between boreholes and meteorological stations, 2) differences of heat transfer in the two systems, convective and radiative in the atmosphere and conductive in the subsurface, 3) complexities of processes at the ground surface, and 4) simplicity of our model (Equation 1-2 and 1-3) that cast comparisons in terms of temperature only. Between 1978 and 2007, these models explain 79, 89, and 95% of the variance for GC-1, SI-1, and DM-1, respectively. Part of the reason for the success of this model is that the ground acts as a low pass filter attenuating high frequency processes that may be perturbing the relationship between air and ground temperatures. Another reason for the apparently good fits may be the dry desert conditions that characterize these sites with little annual precipitation.

It is interesting to note that the greatest misfit occurs at GC-1 where the borehole and meteorological station are collocated. Because linear trends from GC-1 are similar to those from SI-1 and DM-1, we can rule out anomalous warming at GC-1. Additionally, noise in the borehole temperature measurements at GC-1 is smaller than at SI-1 and DM-1. We attribute the relatively larger misfits between GC-1 and EPO to microclimatological effects that may be due to its location near the northeast edge of the Great Salt Lake. These micrometeorological effects prompted us to install EPO in 1993 and are the subject of ongoing studies.

Repeated temperature logging studies such as this should be expanded to a greater diversity of geographic settings to explore the impact of other processes such as the latent heat of freezing and thawing, and evapotranspiration. These studies could also benefit

from a full description of the energy balance at the land surface over decade and longer time scales.

Conclusions

Measurement and analysis of repeat temperature-depth logs from three boreholes in northwest Utah lead to the following conclusions:

1) Temperature measurements at boreholes GC-1, SI-1, and DM-1 made over a 29-year time span provide observational constraints for understanding the relationship between ground and air temperatures. Over the period of observation, both ground and air temperatures are warming.

2) Synthetic temperature profiles calculated from nearby SAT records closely fit observed temperature-depth profiles measured between 1978 and 2007 by matching both the amplitude and pattern of subsurface transient changes. A comparison with forward continued ground temperatures indicates that the observed profiles can be understood in terms of a changing surface temperature.

3) Differences between temperature logs isolate transient variations in ground temperature that can be ascribed to changes in GST.

4) Our direct observation of transient temperatures in boreholes, and comparisons between repeated temperature-depth profiles and SAT records, offer strong support for using GST histories to complement SAT data and multiproxy reconstructions in climate change studies.

Acknowledgments

This project was funded through National Science Foundation grants EAR-0126029 and ATM-0823516 to DSC, and ATM-0823519 to RNH. We also thank all those who participated in logging trips over the course of the study. We appreciate the comments of two anonymous reviewers who helped us better communicate the results of this study.

References

Bartlett, M. G., D. S. Chapman, and R. N. Harris (2006), A decade of ground-air temperature tracking at Emigrant Pass Observatory, Utah, *J. Climate*, 19, 3722–3731.

Beck, A. E. (1982), Precision logging of temperature gradients and the extraction of past climate, *Tectonophysics*, 83, 1–11.

Beltrami, H. (2002), Earth's long-term memory, *Science*, 297, 206–207, doi:10.1126/science.1074027.

Beltrami, H., J. F. González-Rouco, and M. B. Stevens (2006), Subsurface temperatures during the last millennium: Model and observation, *Geophys. Res. Lett.*, 33, L09705, doi:10.1029/2006GL026050.

Chapman, D. S., D. D. Blackwell, W. T. Parry, W. R. Sill, S. H. Ward, and J. A. Whelan (1978), Regional heat flow and geochemical studies in southwest Utah, Final Report, Vol. II, 14-08-0001-G-341, Univ. of Utah, Salt Lake City.

Chapman, D.S., and R. N. Harris (1993), Repeat temperature measurements in borehole GC-1, northwestern Utah: Towards isolating a climate-change signal in borehole temperature profiles, *Geophys. Res. Lett.*, 20, 1891–1894.

Chisholm, T.J., and D. S. Chapman (1992) Climate change inferred from analysis of borehole temperatures; an example from western Utah, *J. Geophys. Res.*, 97, 14,155–14,175.

González-Rouco, F., H. von Storch, and E. Zorita (2003), Deep soil temperature as proxy for surface air-temperature in a coupled model simulation of the last thousand years, *Geophys. Res. Lett.*, 30(21), 2116, doi:10.1029/2003GL018264.

González-Rouco, J. F., H. Beltrami, E. Zorita, and H. von Storch (2006), Simulation and inversion of borehole temperature profiles in surrogate climates: Spatial distribution and surface coupling, *Geophys. Res. Lett.*, 33, L01703, doi:10.1029/2005GL024693.

González-Rouco, J. F., H. Beltrami, E. Zorita, and M. B. Stevens (2009), Borehole climatology: a discussion based on contributions from climate modeling, *Climate of the Past*, 5, 97–127.

Harris, R. N. (2007), Variations in air and ground temperature and the POM-SAT model: results from the Northern Hemisphere, *Climate of the Past*, 3, 611–621.

Harris, R. N., and D. S. Chapman (1995), Climate change on the Colorado Plateau of eastern Utah inferred from borehole temperatures, *J. Geophys. Res.*, 100, 6367–6381.

Harris, R. N., and D. S. Chapman (2001), Mid-latitude (30°-60°N) climatic warming inferred by combining borehole temperatures with surface air temperatures, *Geophys. Res. Lett.*, 28, 747–750.

Harris, R. N., and D. S. Chapman (2005), Borehole temperatures and tree-rings: Seasonality and estimates of extratropical Northern Hemispheric warming, *J. Geophys. Res.*, 110, F04003, doi:10.1029/2005JF000303.

Harris, R. N., and D. S. Chapman (2007), Stop-go temperature logging for precision applications, *Geophysics*, 72 (4), E119–E123, doi:10.1190/1.2734382.

Huang, S. P., H. N. Pollack, and P. –Y. Shen (2000), Temperature trends over the past five centuries reconstructed from borehole temperatures, *Nature*, 403, 756–758.

Karl, T. R., C. N. Williams, Jr., and F. T. Quinlan (1990), United States Historical Climatology Network (HCN) Serial Temperature and Precipitation Data, ORNL/CDIAC-30, NDP-019/R1, Carbon Dioxide Information Analysis Center, Oak Ridge National Laboratory, U.S. Department of Energy, Oak Ridge, Tennessee.

Kooi, H. (2008), Spatial variability in subsurface warming over the last three decades; insight from repeated borehole temperature measurements in The Netherlands, *Earth Planet. Sci. Lett.*, 270, 86–94, doi:10.1016/j.epsl.2008.03.015.

Lachenbruch, A. H., and B. V. Marshall (1986), Climate change: Geothermal evidence from permafrost in the Alaskan Arctic, *Science*, 234, 689–696.

Lewis, T. J., and K. Wang (1992), Influence of terrain on bedrock temperatures, *Global Planet. Change*, 6, 87–100.

Majorowicz, J., and J. Safanda (2005), Measured versus simulated transients of temperature logs—a test of borehole climatology, *J. Geophys. Eng.*, 2, 291–298.

Menne, M.J., C.N. Williams Jr., and R.S. Vose (2009), The United States Historical Climatology Network Monthly Temperature Data - Version 2, *Bull. Amer. Meteor. Soc.,* 90, 993–1007, doi: 10.1175/2008BAMS2613.1.

Pollack, H. N., and D. S. Chapman (1993), Underground records of changing climate, *Scientific American*, June Issue, 46–52.

Pollack, H. N., and S. Huang (2000), Climate reconstruction from subsurface temperatures, *Annu. Rev. Earth Planet. Sci.,* 28, 339–365.

Pollack, H. N., and J. E. Smerdon (2004), Borehole climate reconstructions: Spatial structure and hemispheric averages, *J. Geophys. Res.*, 109, D11106, doi:10.1029/2003JD004163.

Pollack, H. N., J. E. Smerdon, and P. E. van Keken (2005), Variable seasonal coupling between air and ground temperatures: A simple representation in terms of subsurface thermal diffusivity, *Geophys. Res. Lett.,* 32, L15405, doi:10.1029/2005GL023869.

Putnam, S. N., and D. S. Chapman (1996), A geothermal climate change observatory: First year results from Emigrant Pass in Northwest Utah, *J. Geophys. Res.,* 101, 21,877–21,890.

Safanda, J., D. Rajver, A. Correia, and P. Dedecek (2007), Repeated temperature logs from Czech, Slovenian and Portuguese borehole climate observatories, *Climate of the Past,* 3, 453–462.

Smerdon, J. E., H. N. Pollack, V. Cermak, J. W. Enz, M. Kresl, J. Safanda, and J. F. Wehmiller (2004), Air-ground temperature coupling and subsurface propagation of annual temperature signals, *J. Geophys. Res.,* 109, D21107, doi:10.1029/2004JD005056.

Smerdon, J. E., H. N. Pollack, V. Cermak, J. W. Enz, M. Kresl, J. Safanda, and J. F. Wehmiller (2006), Daily, seasonal, and annual relationships between air and subsurface temperatures, *J. Geophys. Res.*, 111, D07101, doi:10.1029/2004JD005578.

Stevens, M. B., J. F. González-Rouco, and H. Beltrami (2008), North American climate of the last millennium: Underground temperatures and model comparison, *J. Geophys. Res.*, 113, F01008, doi:10.1029/2006JF000705.

Stieglitz, M. and J. E. Smerdon (2007), Characterizing land-atmosphere coupling and the implications for subsurface thermodynamics, *J. Climate*, 20, 21-37.

CHAPTER 2

SUBSURFACE THERMAL AND HYDROLOGICAL CHANGES BETWEEN A FORESTED AND A CLEAR-CUT SITE IN THE OREGON CASCADES

Abstract

We report a comparison of temperature and related observations between a set of paired meteorological stations at the Soapgrass Mountain site, Santiam Pass, Cascades Mountains, Oregon, USA. This site contains two separate meteorological towers; one under the old-growth coniferous forest canopy and the other in a nearby opening or clear-cut. The open area has warmer air and soil temperatures and receives greater amounts of incoming radiation. These conditions are contrasted with the muted conditions under the forest canopy. A comparison of the sites shows that between 2000 and 2004, differences in air temperature decrease from 1.7 °C to 1.1 °C. Ground temperature differences are nearly cut in half in the leaf litter from 2.8 °C to 1.5 °C over the same time period. We link this change directly to the change in incoming radiation, with an observed decrease from 295 μmol m^{-2} sec^{-1} to 233 μmol m^{-2} sec^{-1}, that is a result of the forest regrowth at the open area site. Subsurface temperatures are reproducible at the open area site using the Noah land surface model, but larger discrepancies exist at the mature forest site. At

the mature forest site, the incoming solar radiation is too low to reproduce the observations using the Noah land surface model. Using the incoming solar radiation from the open area allows for much better agreement between the Noah model results and the observations.

Introduction

Interactions between the main components of the climate system that include the atmosphere, hydrosphere, cryosphere, lithosphere, and biosphere produce the surface conditions in which we live. Of particular importance are the magnitude and variation in the fluxes of energy and water. These flux variations are dependent on the energy the Earth receives from the Sun, and vary on time scales ranging from daily, yearly, and longer cycles.

At the boundary between the ground and the atmosphere, the flux of energy is largely due to variations in surface air temperature. These variations in surface air temperature can be correlated with subsurface temperatures [e.g., *Lachenbruch and Marshall*, 1986; *Putnam and Chapman*, 1996]. The analysis of subsurface temperature variations can be understood through the physics of heat diffusion [e.g., *Carslaw and Jaeger*, 1959; *Turcotte and Schubert*, 2002] and therefore is unique among the methods used to reconstruct paleotemperature [*Bradley*, 1999; *National Research Council*, 2006]. As such, subsurface temperatures are a rich source of information about how ground temperatures have changed in the past as well as the energy balance at the boundary layer between Earth's surface and the atmosphere [e.g., *Beltrami*, 2002].

Modeling studies suggest that variations in precipitation can have an important influence on variations in ground temperatures [*Lin et al.*, 2003; *Pollack et al.*, 2005; *Zhang et al.*, 2005] while observatory based data tend to show this effect is of modest importance [*Bartlett et al.*, 2004, 2005; *Smerdon et al.*, 2003]. The Oregon Cascades are a locality where these studies can be tested, since topographic uplifting of moisture-laden air from the Pacific results in rain events that are of long duration and low intensity [*Bierlmaier and McKee*, 1989].

The Pacific Northwest is a climatically sensitive area where continued warming is predicted to induce a switch from a snow-dominated to a rain-dominated winter precipitation regime [*Mote et al.*, 2005; *Stoelinga et al.*, 2010] with a likely impact on the subsurface thermal regime. Additionally, the impact of land cover change through deforestation on this system is poorly known but is likely to amplify subsurface warming [*Nitoiu and Beltrami*, 2005]. In this study, we use existing meteorological data in the Cascades of Oregon first to understand, document, and compare the differences between closely paired stations of differing land cover, and second, to test and evaluate a widely used Land Surface Model (LSM) against the observations collected from geographically close, yet strongly differing in land cover, sites.

Data come from one paired meteorological site established in 1998 by the Environmental Protection Agency. Meteorological data include air temperature, humidity, wind speed and direction, short wave incoming radiation, snow depth, and precipitation; soil data consist of ground temperature and soil moisture. The meteorological data at the site were used as the atmospheric forcing to drive the Noah LSM [*Mahrt and Pan*, 1984; *Pan and Mahrt*, 1987; *Chen et al.*, 1996; *Chen and Dudhia*,

2001a; *Ek et al.*, 2003]. The Noah LSM grew out of joint efforts between the National Centers for Environmental Prediction, Oregon State University, the Air Force Weather Agency, and the Hydrologic Research Laboratory and is a multilayer soil and vegetation model that can be used in either "coupled" or "offline" modes. In coupled mode, the Noah LSM (and other LSMs) is used to describe the surface properties, along with the fluxes of heat, moisture, and momentum, that are used as the lower boundary conditions in numerical weather prediction (NWP) models such as the Weather Research and Forecasting (WRF) Model [*Skamarock et al.*, 2005; 2008] or the Mesoscale Meteorology (MM5) Model [*Dudhia*, 1993; *Chen and Dudhia*, 2001b]. In offline mode, the Noah LSM is used as a stand-alone, one-dimensional column with near-surface atmospheric data providing the forcing input for the model to examine single-site land-surface simulations. The Noah LSM is known to be both robust and successful in semiarid climate regions such as the U.S. Great Plains in both Kansas and Nebraska [*Chen et al.*, 1996; *Evans et al.*, 2005; *Radell and Rowe*, 2008] and Southwest in southeastern Arizona [*Hogue et al.*, 2005], but has known shortcomings in mountainous regions where precipitation comes largely in the form of snow [*Sheffield et al.*, 2003; *Barlage et al.*, 2010].

Our key for understanding water and energy fluxes across the land surface interface at the Soapgrass Mountain site is to concentrate on the differences and similarities between the open and closed canopy sites. Questions we address include: 1) What is the impact of differences in incoming short wave radiation, particularly during summer months, between forested and cleared sites on ground temperature and soil moisture at each site? 2) How does the pattern of snow accumulation and ablation differ

between cleared and forested sites and what is the impact on soil moisture and ground temperature? 3) What is the impact of precipitation on ground temperature and soil moisture? 4) By comparing forested and open sites, how will continued warming and land cover change affect subsurface temperatures? 5) Does the Noah LSM accurately predict subsurface temperatures and soil moisture conditions?

Field Site

The field site at Soapgrass Mountain was established by the Environmental Protection Agency in 1998 in an effort to provide data for and to test performance of a biogeochemical model to understand plant growth and its relation to meteorological conditions [*Beedlow et al.*, 2007]. This paired site is located on the western slope of the Cascade Mountains in central Oregon (Figure 2-1; 44.346 °N, 122.290 °W). The elevation is 1190 m for the forested site and 1206 m for the open site. The two sites are a distance of 0.38 km apart and part of a larger network that represents a wide range of temperature, precipitation, soil properties, and plant productivity. Each site in the network established a pair of metrological towers with one of the pairs being under the forest canopy and the other in a nearby opening or clear-cut area (Figure 2-2). The site within the forest provides information on the weather and soil conditions under the canopy and provides the best estimate of the influence of the canopy on soil moisture and soil temperature. The site in the opening or clear-cut provides the best estimate on the overall weather conditions for the area and provides data on the soil temperature and moisture conditions not influenced by the forest canopy. These open area observations also serve as a proxy for the radiation, air temperature, and precipitation at the top of the

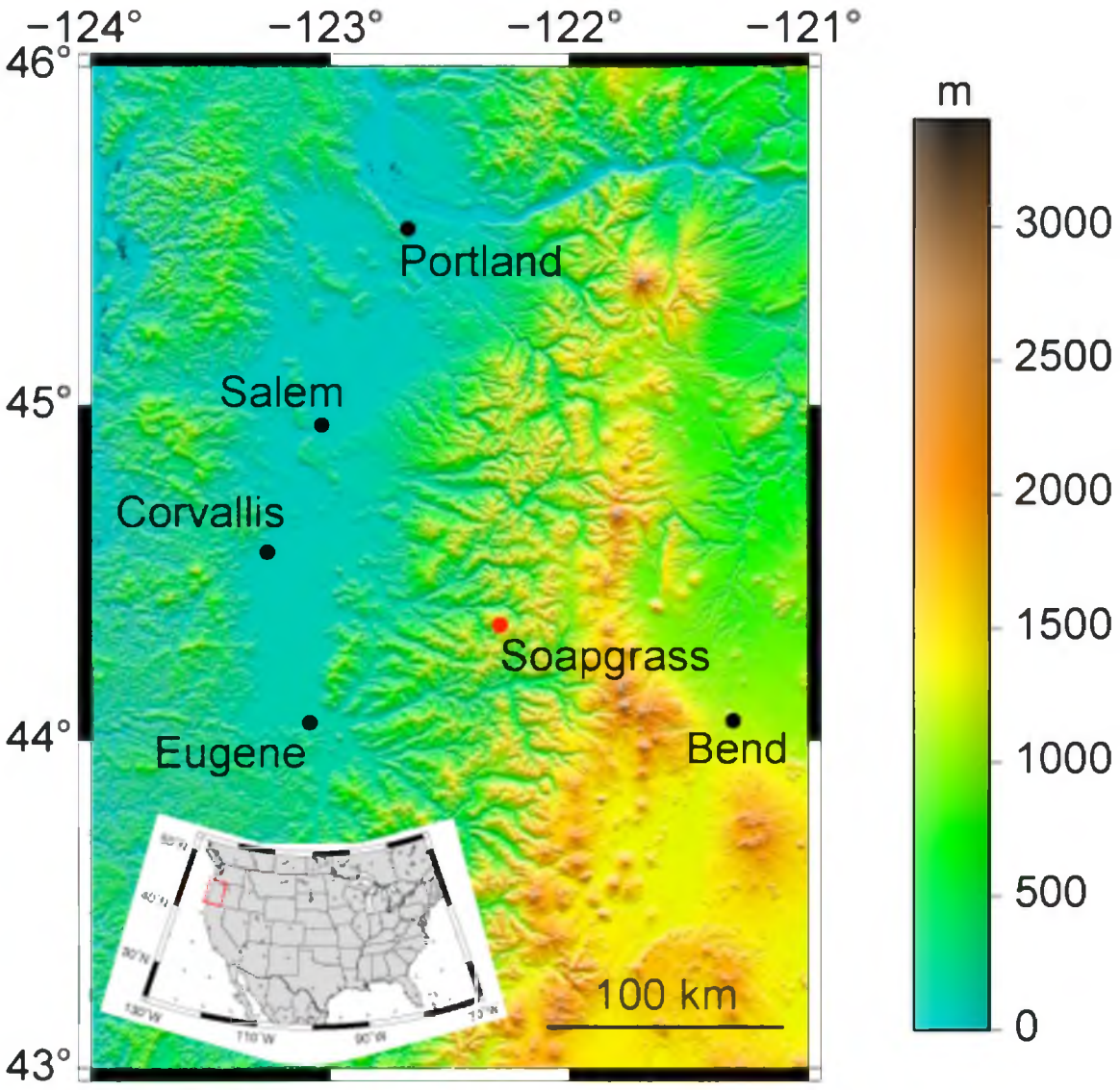

Figure 2-1. Site location of the paired meteorological stations at Soapgrass Mountain in the Cascade Mountains, Oregon, USA. Background map colors represent elevation above sea level (meters).

Figure 2-2. Photographs of the Soapgrass Mountain site showing the contrast between the open (top) and closed (bottom) canopy locations.

forest canopy for the mature forest area. In the selection of the open or clear-cut site metrological towers, the objective was to select a nearby site that was similar in both elevation and aspect to the forested site and was large enough so that the tower was not shaded or affected by the surrounding vegetation.

The same basic weather and soil monitoring sensors were installed at each site and are listed in Table 2-1. The instrument package at each site measures air temperature, humidity, wind speed, photosynthetically active radiation (PAR), precipitation, snow depth, soil temperature, and soil moisture. Soil temperature and volumetric soil moisture are measured at several depths (Table 2-1). There are occasional gaps in the data due to equipment failure or to offsets in timing due to instrumentation installation.

Site Descriptions

Soapgrass Mountain Open Area (SMOA). Average daily air temperature at the SMOA (Figure 2-3a) site ranges between a minimum of -5.5 °C in 2002 and a maximum of 25.7 °C in the year 2004. A spread of approximately 20 °C between the maximum and minimum daily average air temperature is fairly consistent throughout the time period of our observations. The annual average air temperature varied between 7.7 °C in the year 2000 and 8.4 °C in the year 2003 (Table 2-2).

The annual average relative humidity at the SMOA during our observational period is between 72.7 and 77.4% (Table 2-2), with an average daily minimum of 11.3% and a maximum of 100% (Figure 2-3b). The precipitation averaged between 3.9 and 5.4

Table 2-1. Listing of weather and soil sensors at Soapgrass Mountain.

Aboveground sensors	Units
Air temperature	°C
Relative humidity	%
Photosynthetically Active Radiation (PAR)	µmol m^{-2} sec^{-1}
Precipitation	mm hr^{-1}
Wind speed	m sec^{-1}
Snow depth	cm
Belowground Sensors	
Soil temperature @ litter, 5, 15, 30 cm	°C
Soil moisture @ surface, 0-20, 20-40, 40-60 cm	%

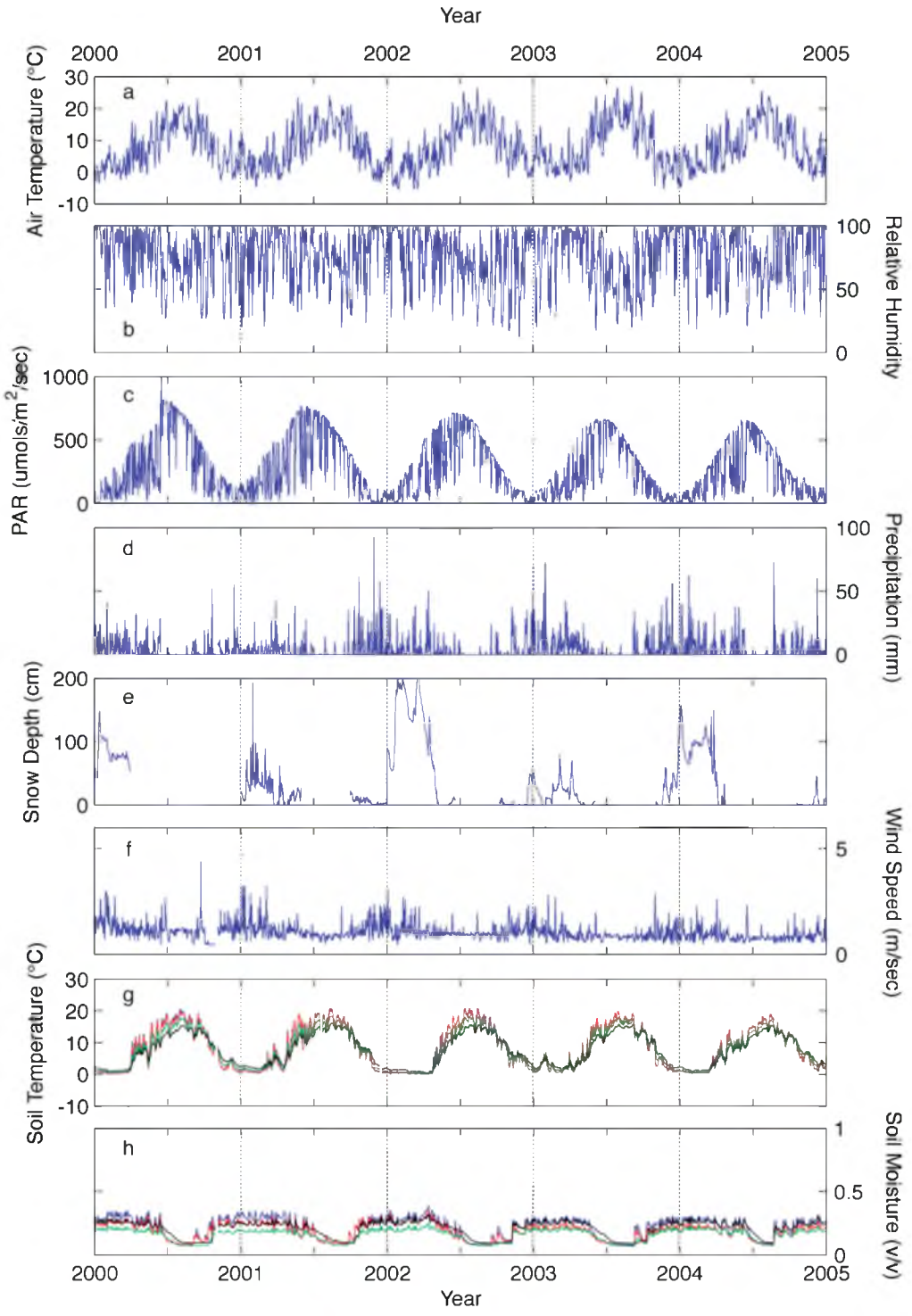

Figure 2-3. Meteorological and subsurface data observed at the Soapgrass Mountain Open Area (SMOA). a) Air temperature. b) Relative humidity. c) Photosynthetically active radiation. d) Precipitation. e) Snow depth. f) Wind speed. g) Soil temperature (blue is the litter temperature, red is 5 cm, green is 15 cm, and black is 30 cm. h) Soil moisture (blue is surface soil moisture, red is 0-20 cm, green is 20-40 cm, and black is 40-60 cm).

Table 2-2. Annual averages of meteorological and subsurface data at the Soapgrass Mountain Open Area.

	Units	2000	2001	2002	2003	2004
Air Temperature	°C	7.7	7.9	7.9	8.4	8.3
Relative Humidity	%	76.2	75.9	72.7	74.8	77.4
PAR	µmol m^{-2} sec^{-1}	304.1	307.4	288.6	249.4	239.6
Rain	mm day^{-1}	4.4	4.5	3.9	5.4	5.1
Snow Depth	cm	37.0	18.1	66.3	19.3	45.8
Wind Speed	m sec^{-1}	1.2	1.1	1.1	0.9	0.9
Ground Temperature						
Litter	°C	8.3	8.8	7.9	8.1	7.8
5 cm	°C	8.1	8.7	7.8	8.2	7.8
15 cm	°C	7.8	8.4	7.5	7.9	7.6
30 cm	°C	7.4	8.1	7.2	7.7	7.5
Soil Moisture						
Surface	%	22.8	22.4	21.2	20.8	22.7
0-20 cm	%	19.9	20.1	18.7	16.9	18.3
20-40 cm	%	15.7	15.8	15.5	15.7	17.2
40-60 cm	%	20.3	20.6	20.0	19.9	22.3

mm per day (Table 2-2), with a daily range between 0 mm to 92 mm per day (Figure 2-3d). Little to no rain occurred from June through August in all years. This time corresponds with the highest ground temperatures and the lowest soil moisture and relative humidity. Soil moisture varied between 7 and 35% of saturation on a daily basis (Figure 2-3h), with an annual average at the surface between 20.8 and 22.8% (Table 2-2). Soil moisture is positively correlated with precipitation events (Figure 2-4a). Interestingly, the soil moisture in the depth range of 20-40 cm was consistently lower than that measured from 40-60 cm (Table 2-2).

PAR at the SMOA slowly increases from winter through spring until the summer when it dramatically rises before falling again into the winter (Figure 2-3c). The maximum of the PAR occurs when the precipitation is at a minimum, relative humidity is generally lower, and the air temperature is highest (Figure 2-3). During the summer, more solar radiation is able to get to the ground than in the remainder of the year when days are more likely to be wet and overcast. Over the course of our observation (2000 – 2004), daily maximum PAR can be seen to decrease (Figure 2-3c) from ~820 μmol m^{-2} s^{-1} in 2000 to ~650 μmol m^{-2} s^{-1} in 2004. Annual averages of PAR also decrease over this time period from 304 μmol m^{-2} s^{-1} in 2000 to ~240 μmol m^{-2} s^{-1} in 2004 (Table 2-2). This can be directly related to the regrowth of vegetation at the site over this time.

Wind speed at SMOA averages 1.2 m s^{-1} with gusts up to 5.9 m s^{-1} (Figure 2-3f). Further, as with PAR, annual average wind speed shows a slight decrease over the time of our observations from 1.2 to 0.9 m s^{-1} (Table 2-2).

Precipitation at SMOA only occurred when the air temperature was between -2 to 15 °C. Precipitation at the lower temperatures resulted in snow. The snow depth

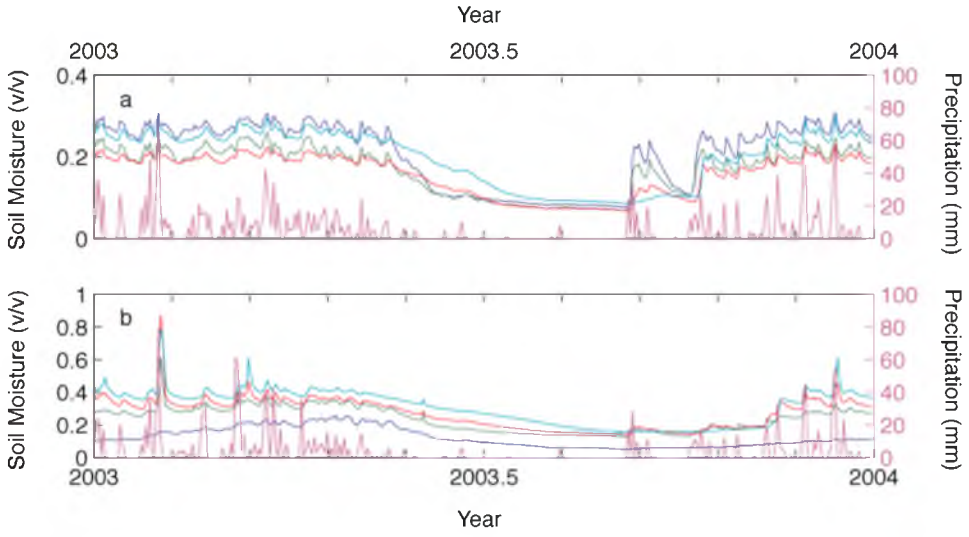

Figure 2-4. Soil moisture (blue is surface soil moisture, red is 0-20 cm, green is 20-40 cm, and black is 40-60 cm) and precipitation (magenta) observed at a) the Soapgrass Mountain Open Area and b) the Soapgrass Mountain Mature Forest during the year 2003.

maximum of 214 cm occurred in 2002, with most years having only a few days of more than 100 cm of snow (Figure 2-3e). Snow remained at the site until late March or early April, and was present at air temperatures up to 15 °C. While snow was on the ground, ground temperatures remained just above freezing. After the loss of snow, ground temperatures were observed to increase. The increase and subsequent change in ground temperatures followed changes in the air temperature, albeit attenuated and lagged as expected from the diffusive process.

Average ground temperatures were observed to decrease from the leaf litter to a depth of 30 cm in all years except for 2003 (Table 2-2). The range of temperatures also decreased in each depth interval from 0 to 25 °C in the litter to 0.3 to 16.3 °C at 30 cm (Figure 2-3g). The temperature range in the litter was less than that measured in the air temperature, and also had a lower maximum temperature than was measured in the air. Initially, the average ground temperature in the upper 15 cm was greater than the average air temperature; however, beginning in 2002, the average air temperature was higher than the ground temperature (Table 2-2). This reversal corresponds to a slight decrease in the amplitude of the ground temperatures over our observational time period, which we attribute to be caused by the decrease in PAR.

Soapgrass Mountain Mature Forest (SMMF). The average daily air temperature at the SMMF (Figure 2-5a) ranges between -6.3 and 24.7 °C. Overall, the minimum temperature measured -8.3 °C while the maximum temperature was 30.5 °C. The annual average air temperature increased from 6.0 to 7.2 °C over our observational period (Table 2-3).

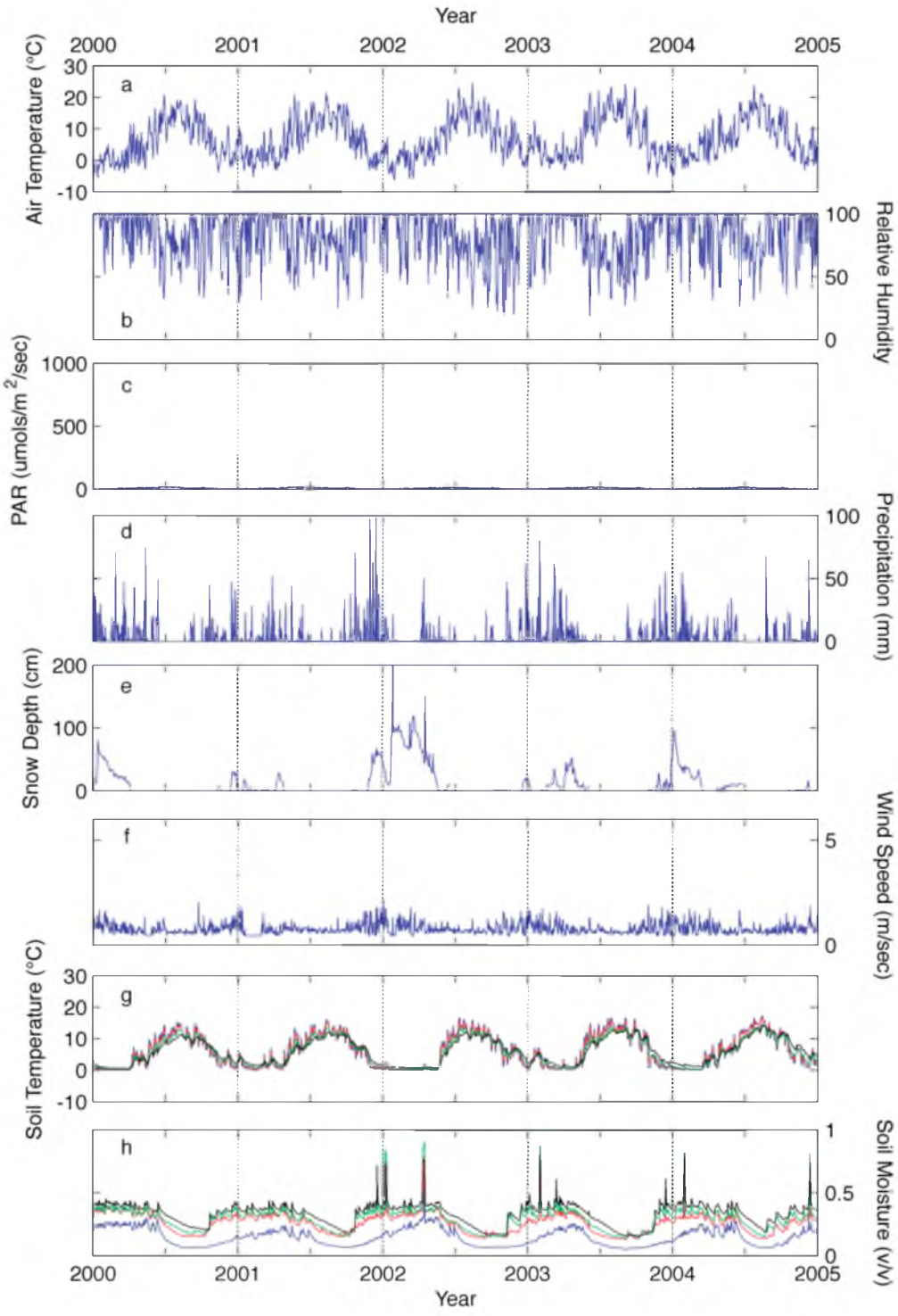

Figure 2-5. Meteorological and subsurface data observed at the Soapgrass Mountain Mature Forest (SMMF). a) Air temperature. b) Relative humidity. c) Photosynthetically active radiation. d) Precipitation. e) Snow depth. f) Wind speed. g) Soil temperature (blue is the litter temperature, red is 5 cm, green is 15 cm, and black is 30 cm. h) Soil moisture (blue is surface soil moisture, red is 0-20 cm, green is 20-40 cm, and black is 40-60 cm).

Table 2-3. Annual averages of meteorological and subsurface data at the Soapgrass Mountain Mature Forest.

	Units	2000	2001	2002	2003	2004
Air Temperature	°C	6.0	6.8	6.6	7.2	7.2
Relative Humidity	%	83.7	82.1	79.4	81.3	82.6
PAR	µmol m^{-2} sec^{-1}	7.1	7.1	5.6	6.9	6.3
Rain	mm day^{-1}	4.4	4.3	2.5	4.3	3.8
Snow Depth	cm	17.5	6.2	37.3	10.7	14.4
Wind Speed	m sec^{-1}	0.8	0.8	0.8	0.8	0.8
Ground Temperature						
Litter	°C	5.5	6.1	5.6	6.3	6.4
5 cm	°C	5.5	6.2	5.6	6.3	6.5
15 cm	°C	5.3	6.0	5.4	6.0	6.1
30 cm	°C	5.1	6.0	5.5	6.3	6.8
Soil Moisture						
Surface	%	16.2	13.4	15.6	12.3	15.6
0-20 cm	%	28.2	26.4	25.6	23.7	25.7
20-40 cm	%	30.3	29.1	28.8	27.2	29.9
40-60 cm	%	34.1	33.4	32.4	31.0	35.1

The annual average relative humidity at the SMMF was between 79.4 and 83.6% (Table 2-3), with a daily average minimum of 18.9% and a maximum of 100% (Figure 2-5b). Relative humidity minimums correspond with high air temperatures in the summer (Figure 2-5b).

Shade from trees in the SMMF accounts for little to no PAR measured at the surface with a daily average maximum of only 34.1 μmol m^{-2} s^{-1} measured at the site (Figure 2-5c) and annual averages ranging between 5.6 and 7.1 μmol m^{-2} s^{-1} (Table 2-3). Hence, the tall trees absorb the majority of the incoming PAR and little can be utilized by vegetation at the ground level (Figure 2-2).

Precipitation at the SMMF was between 0 and 97.9 mm a day (Figure 2-5d) while the annual average was between 2.5 and 4.3 mm a day (Table 2-3). Maximum snow depth of over 150 cm occurred in 2002, but most years, the high was well below 100 cm (Figure 2-5e).

Wind speed in the SMMF was never very high due to the trees, with a daily average maximum of 2.1 m s^{-1} (Figure 2-5f) and annual averages less than 0.8 m s^{-1} (Table 2-3). Wind speeds were generally higher during the winter (Figure 2-5f).

Ground temperatures at SMMF remained near zero while snow was on the ground, and then followed the pattern seen in the air temperature but with attenuated amplitudes and a phase lag (Figure 2-5g). The average annual SMMF air temperature was higher than the average ground temperature measured at all depths by between 0.4 to 1.2 °C (Figure 2-5g; Table 2-3). The range of ground temperatures decreased with depth from a low of 0 °C to a high of 17.2 °C in the litter and from 0.5 °C to 14.1 °C at a depth of 30 cm.

Soil moisture at SMMF increase with depth for all years during our observations from an average as low as 12.3% at the surface to 28.2% to as high as 35.1% from 40-60 cm (Figure 2-5h; Table 2-3). Soil moisture increases are observed to follow precipitation events (Figure 2-4b). Further, several spikes in the soil moisture are observed in the winter beginning in 2002 and are perhaps associated with heavy precipitation, rapid snowmelt, and infiltration. Oddly, the spikes are only seen in the bulk soil moisture observations and not in the surface measurement. In general, the ground temperatures are insulated by snow on the ground during these soil moisture spikes (Figure 2-5g and 2-5h), but during the winter of 2003, the soil temperature was almost 7 °C just after a large (>50 mm) precipitation event that resulted in a spike in soil moisture as high as 87.4% between 20-40 cm depth (Figure 2-6). Soil moisture levels return quickly to background levels after the heavy precipitation (Figure 2-6).

Comparison of Soapgrass Mountain sites. A comparison between the open area and the mature forest is made in Figure 2-7 (and Table 2-4) by plotting the difference (SMOA – SMMF) for eight parameters over the five-year recording period. Air temperature at Soapgrass Mountain is initially 1.7 °C warmer in the open area, but the difference decreases to 1.1 °C (Figure 2-7a; Table 2-4). The warmer open area air temperatures are largely due to the differences between the cooling provided by the large, mature trees in the SMMF. Humidity levels in the open area rarely exceed humidity in the mature forest, and are lower in the open area by 7.2% in 2000, although it is not constant throughout the year (Figure 2-7b). The relative humidity difference decreases to only 5.2% by 2004 (Table 2-4). The difference in PAR measured at the two sites is

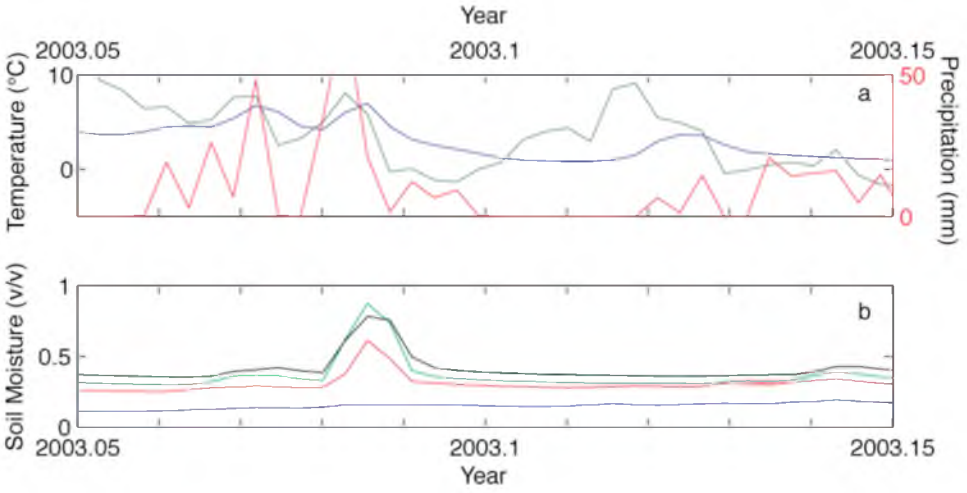

Figure 2-6. Precipitation, temperatures, and soil moisture at the Soapgrass Mountain Mature Forest associate with a heavy precipitation event in 2003. a) Precipitation (red), air temperature (green), and litter temperature (blue) at the Soapgrass Mountain Mature Forest near the beginning of 2003. b) Soil moisture rise associated with the heavy precipitation event. Soil moisture (blue is surface soil moisture, red is 0-20 cm, green is 20-40 cm, and black is 40-60 cm) is observed to rise quickly for all of the subsurface layers. Tick marks represent approximately 3.6 days.

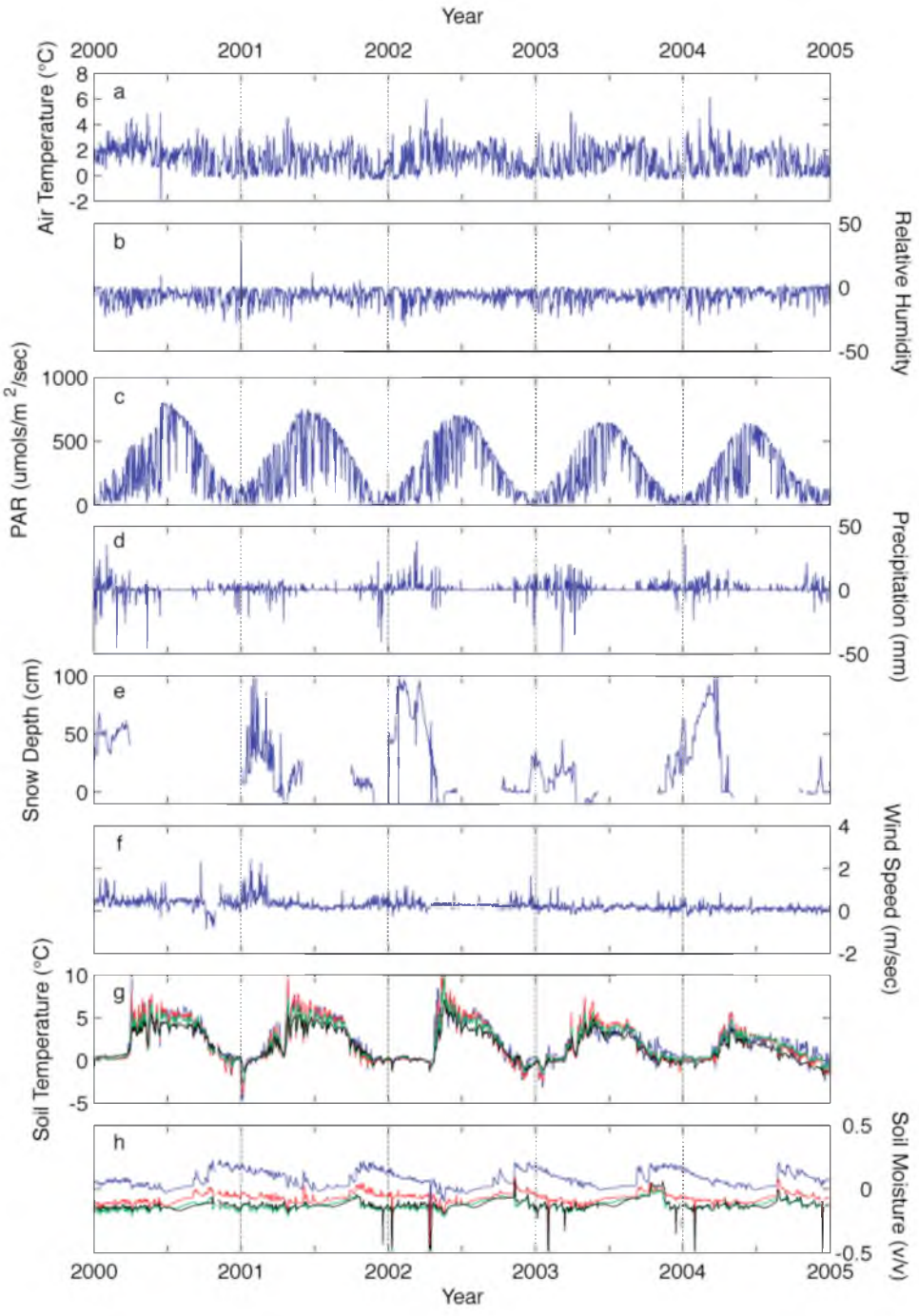

Figure 2-7. Differences of meteorological and subsurface data between the Soapgrass Mountain Open Area and Mature Forest. a) Air temperature. b) Relative humidity. c) Photosynthetically active radiation. d) Precipitation. e) Snow depth. f) Wind speed. g) Soil temperature (where blue is the litter temperature, red is 5 cm, green is 15 cm, and black is 30 cm. h) Soil moisture (where blue is surface soil moisture, red is 0-20 cm, green is 20-40 cm, and black is 40-60 cm).

Table 2-4. Differences between meteorological and subsurface observations at Soapgrass Mountain Open Area and Mature Forest (SMOA – SMMF).

	Units	2000	2001	2002	2003	2004
Air Temperature	°C	1.7	1.1	1.3	1.2	1.1
Relative Humidity	%	-7.2	-6.2	-6.7	-6.5	-5.2
PAR	$\mu mol\ m^{-2}\ sec^{-1}$	294.5	300.2	283.0	242.6	233.3
Rain	$mm\ day^{-1}$	0.0	0.2	1.4	1.1	1.2
Snow Depth	cm	48.7	8.7	29.5	8.6	33.0
Wind Speed	$m\ sec^{-1}$	0.4	0.4	0.3	0.2	0.1
Ground Temperature						
Litter	°C	2.8	2.7	2.3	1.8	1.5
5 cm	°C	2.6	2.5	2.2	1.9	1.3
15 cm	°C	2.5	2.4	2.0	1.9	1.5
30 cm	°C	2.3	2.1	1.7	1.4	0.7
Soil Moisture						
Surface	%	6.4	9.0	5.6	8.5	7.1
0-20 cm	%	-8.4	-6.3	-6.8	-6.9	-7.4
20-40 cm	%	-14.6	-13.3	-13.3	-11.5	-12.7
40-60 cm	%	-13.9	-12.7	-12.5	-11.2	-12.8

nearly identical to the PAR measured at SMOA, since the canopy absorbs nearly all of the PAR before reaching the ground in the SMMF (Figure 2-7c; Table 2-4).

Over the course of the year 2000, the average difference in precipitation between SMOA and SMMF is nearly zero, although there are large differences in individual precipitation events. These differences are primarily during the early portion of the year. For subsequent years, the open area site receives slightly more rain per day (Figure 2-7d; Table 2-4). Snow depth in the open area exceeded that in mature forest each year by up to 100 cm (Figure 2-7e), although the snow remained on the ground in the SMMF after the snow was gone from the SMOA. For example, in 2002, the snow remained on the ground about 11 days longer in the mature forest (Figure 2-8a). Air temperatures in the SMMF during this additional week were lower than the air temperature at SMOA (Figure 2-8b). Litter temperatures at SMMF are observed to be consistent with snow cover (Figure 2-8b), but at SMOA, the ground temperatures warm sooner than would be expected with snow cover. This is most likely due to snow cover above the ground temperature sensors melting earlier than below the snow depth sensor.

Wind speeds were 0.4 m s^{-1} faster in the SMOA than in the SMMF in the year 2000 (Figure 2-7f; Table 2-4), as the forest acts as a barrier to sustained wind. However, over the course of observations, the difference in wind velocity decreases down to 0.1 m s^{-1} as the vegetation growth at the open area begins to block wind (Table 2-4).

Ground temperatures were warmer in the SMOA at all times throughout the year with the exception of the winter when snow was on the ground (Figure 2-7g). During this time, ground temperatures at both sites were essentially the same because the snow insulated the ground to just above freezing. However, once the snow melted, the SMOA

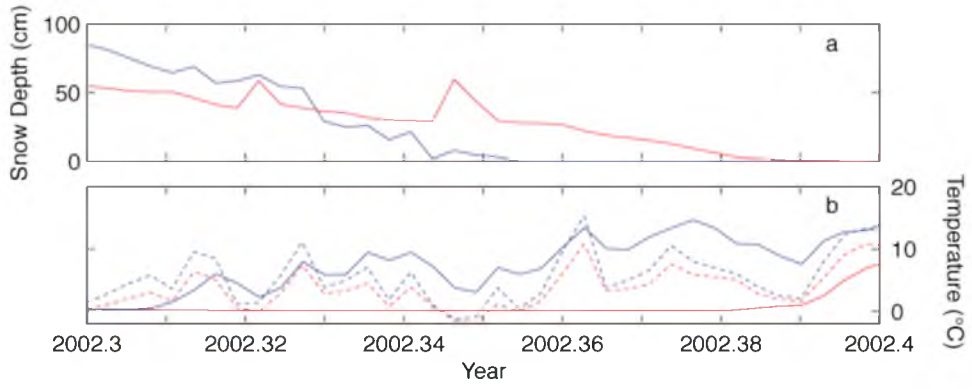

Figure 2-8. Snow depth and temperature change for SMOA and SMMF in 2002. a) Snow depth in early 2002 for SMOA (blue) and SMMF (red). b) Air (dashed) and litter (solid) temperatures at SMOA (blue) and SMMF (red). Tick marks represent approximately 3.6 days.

ground temperatures rapidly warmed at a greater rate than at SMMF (Figure 2-8). Summer ground temperatures were initially around 5 °C warmer at SMOA in 2000 (Figure 2-7g), although this temperature difference decreased between 2000 and 2004 as the open area experienced vegetation regrowth (Figure 2-7g; Table 2-4). Further, the temperature difference decreased at all depths over the course of observation (Table 2-4).

Soil moisture differences were generally small throughout the year (Figure 2-7h; Table 2-4). The most significant difference was that the surface at the SMOA site was between 5.6 and 9% more saturated, but that the subsurface was wetter at SMMF by 6.3 to 14.6% (Table 2-4). Also, surface soil moisture differences were highest in the winter but reduced in the summer (Figure 2-7h).

Land Surface Modeling

We used the public release version 2.7.1 of the Noah LSM [*Ek et al.*, 2003] that is an uncoupled, 1-D column model that can be used to perform single-site land-surface simulations. Using near-surface atmospheric data as input forcing, Noah simulates the soil moisture, soil temperature, skin temperature, snowpack depth, snowpack water equivalent, canopy water content, and the energy flux and water flux terms of the surface energy balance and surface water balance. The atmospheric data necessary for Noah include wind speed, air temperature, relative humidity, precipitation, barometric pressure, and incoming solar and longwave radiation. The stations at the Soapgrass Mountain site measure the first four variables. Barometric pressure was measured at Falls Creek, a site about 8 km away and 660 m lower than Soapgrass Mountain. Although not ideal due to

the difference in elevation, we use the Falls Creek pressure data for the pressure input at the Soapgrass Mountain site.

Incoming solar radiation is measured as photosynthetically active radiation (PAR). PAR is the measure of solar radiation in the range between 400 and 700 nanometers that is necessary for photosynthesis in plants. The Noah LSM requires solar radiation to be in the form of solar irradiance [W m^{-2}], while PAR is in the form of number of photons [μmol m^{-2} s^{-1}]. Therefore, it is necessary to use PAR to estimate the solar irradiance. Unfortunately, no definitive relationship between solar irradiance and PAR exists [e.g., *Udo and Aro*, 1999, and references therein], but conservative estimates indicate that the ratio of ~0.46 – 0.50 (PAR/irradiance) is appropriate for our geographic locality [*Rao*, 1984; *Udo and Aro*, 1999].

Longwave radiation is not measured at our sites, so we use the methodology of *Idso and Jackson* [1969] to estimate the atmospheric emissivity, ε_a, using the air temperature, T, expressed as degrees absolute Kelvin, as

$$\varepsilon_a = 1 - 0.261 exp\left(-7.77 \cdot 10^{-4}\left[273.15 - T\right]^2\right). \qquad (2\text{-}1)$$

The longwave radiation, R, is

$$R = \varepsilon_a \sigma T^4, \qquad (2\text{-}2)$$

where σ is the Stefan-Boltzmann constant (5.67 x 10^{-8} W m^{-2} K^{-4}).

Other required inputs into the Noah LSM include monthly values of green vegetation fraction [*Gutman and Ignatov*, 1998] and snow-free albedo for the simulation site, along with the maximum albedo expected for deep snow [*Robinson and Kukla*, 1985]. Resource maps with these data can be accessed from the National Oceanographic and Atmospheric Administration's Environmental Modeling Center website (http://wwwt.emc.ncep.noaa.gov/?branch=NOAH&tab=fetchmodelconf). Further, information on soil and vegetation type for each site is needed (Table 2-5).

While there is not a set or standard for LSM initialization, it has been shown that it takes many model years to come to hydrologic and thermal equilibrium [*Yang et al.*, 1995], with the Noah LSM generally requiring around five or more years to initialize [e.g., *Shrestha and Houser*, 2010]. We therefore initialized our modeling runs with a ten-year spin-up of the atmospheric forcing data from the complete year 1999 at each site, followed by an analysis and comparison of the model results and observations for snow depth, subsurface temperature, and soil moisture beginning with the year 2000 and going through 2004.

Model results and comparisons. We compare the modeling results of snow depth, subsurface temperature, and soil moisture with our observations of these meteorological variables in Figures 2-9 through 2-13. Snow depth (Figure 2-9) is very poorly modeled for both open and mature forest sites. This misfit is not surprising, as snow cover has been shown to be an issue with the Noah LSM [e.g., *Barlage et al.*, 2010, and references therein]. The difference between observations and model results exceeds 300 cm at SMOA, while the difference is at least 1500 cm during one year at SMMF. This difference is most likely due to the nature of the input parameters or model physics,

Table 2-5. Soil and vegetation parameters at Soapgrass Mountain.

Field Site	Soil Type	Dominant Tree Species[a]	Stand Age (years)	Leaf Area Index[b]
Soapgrass	Coarse sandy loam	PSME, TSHE	>500	6.8±0.8

[a] Tree species abbreviations: PSME – Pseudotsuga menziesii, TSHE – Tsuga heterophylla.
[b] Leaf area index is expressed as the mean and associated standard error for each forested site.

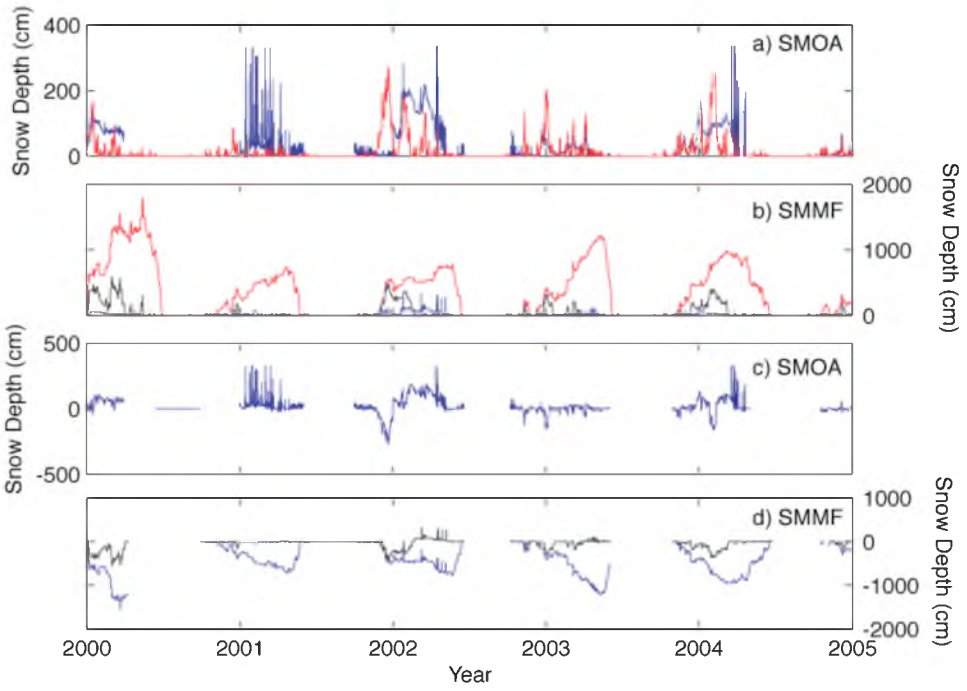

Figure 2-9. Snow depth comparisons. (Top two panels) Snow depth from observations (blue) and modeling results (red) for SMOA and SMMF. Bottom two panels show the difference between the model result and the observations.

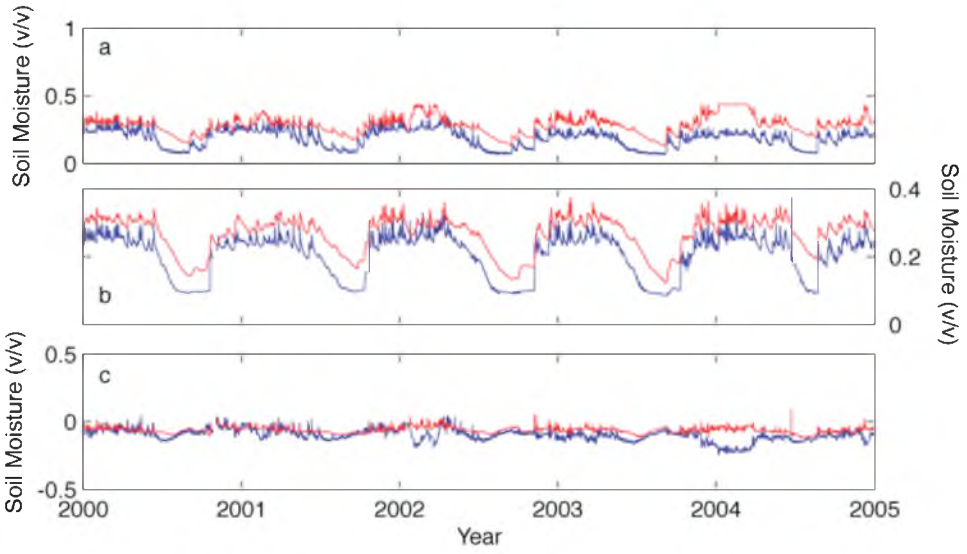

Figure 2-10. Soil moisture from observations (blue) and modeling (red) results for SMOA at a depth of a) 10 cm and b) 50 cm. c) Differences between the observation and model at 10 cm (blue) and 50 cm (red).

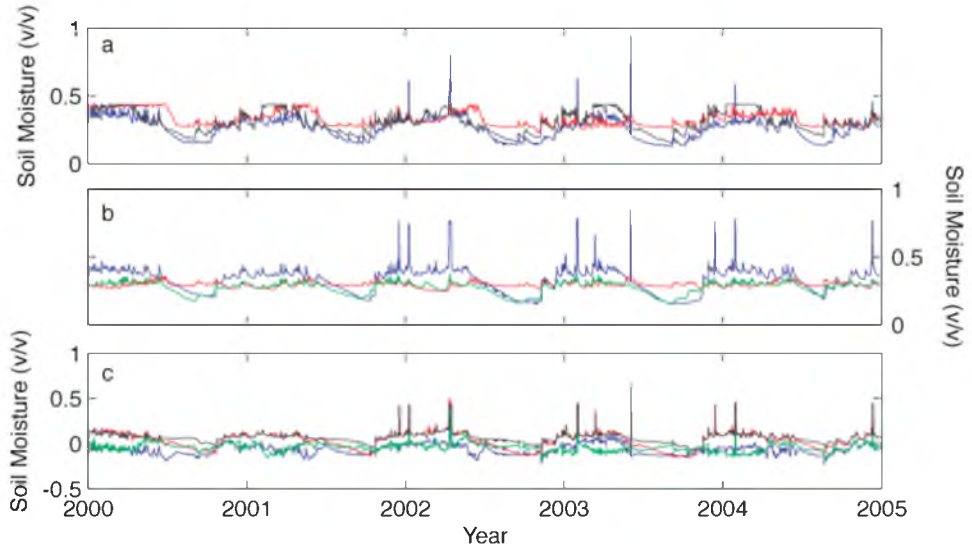

Figure 2-11. Soil moisture from observations (blue) and modeling (red, black, green) results for SMMF at a depth of a) 10 cm and b) 50 cm. The black and green lines represent a model in which the incoming solar radiation forcing is taken from the open area observations. c) Differences between the observation and model at 10 cm (blue, black) and 50 cm (red, green).

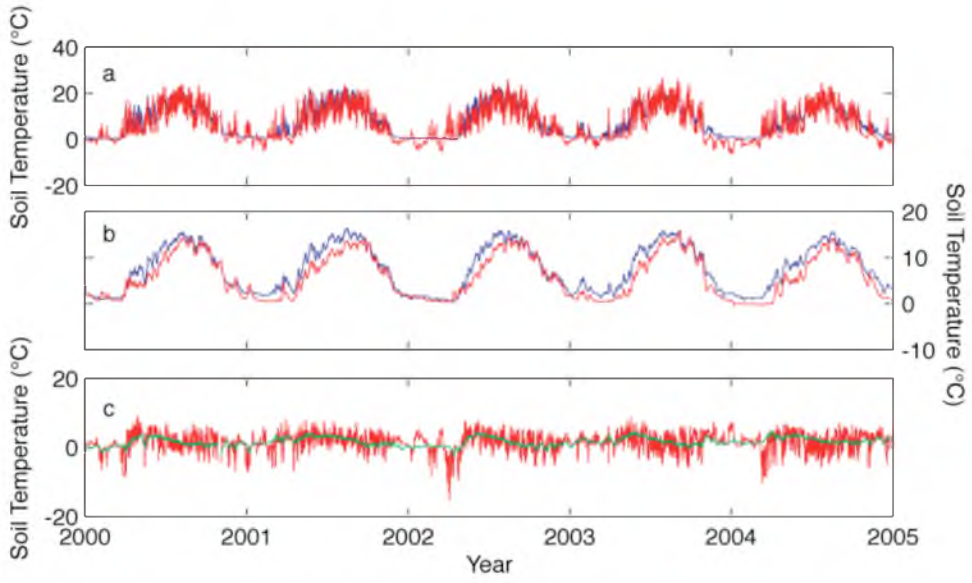

Figure 2-12. Subsurface temperature from observations (blue) and modeling (red) at a depth of a) 5 cm and b) 30 cm for SMOA. c) Differences between the observations and model results at 5 cm (red) and 30 cm (green).

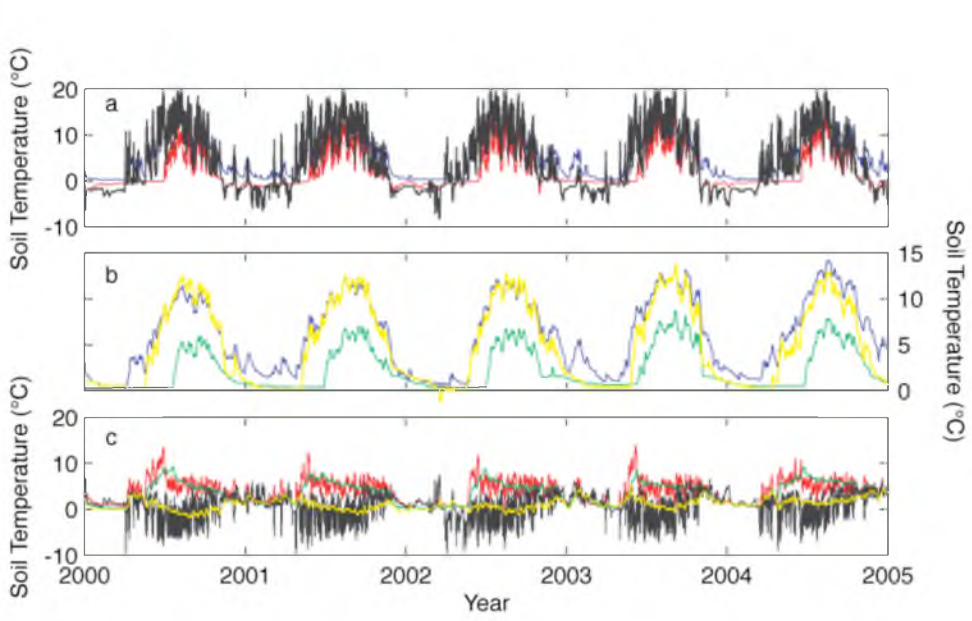

Figure 2-13. Subsurface temperature from observations (blue) and modeling (red, black green and yellow) at a depth of a) 5 cm and b) 30 cm for SMMF. The black and yellow lines represent a model in which the incoming solar radiation forcing is taken from the open area observations. c) Differences between the observations and model results at 5 cm (red, black) and 30 cm (green, yellow).

with lower radiation measured at the surface owing to forest canopy capture (i.e., shading). Onset of snow appears to correspond well between the model and the observations. Snow duration times, however, seem to extend longer into the spring in the model results, particularly at SMMF. These factors have the most impact on correctly modeling the subsurface temperatures [*Bartlett et al.*, 2004; 2005]. Improvement in the fit between observation and model is achieved at SMMF by using the incoming solar radiation forcing from SMOA (black line, Figure 2-9 b and d). This improvement is due to the fact that the measured radiation at the surface of SMMF is extremely low, resulting in abnormally high snow totals. When using radiation from SMOA, snow totals become more reasonable for a site less than 400 meters away.

Soil moisture (Figure 2-10) patterns are matched fairly well at both SMOA and SMMF, although the model produces slightly higher moisture content than what is observed at SMOA. At SMMF (Figure 2-11), the variability of the model results are not as great as the observations. A slight improvement is seen in the modeling results for SMMF when the incoming solar radiation from SMOA is used (Figure 2-11, black and green lines). The model, however, still does not capture the high variability of the observations, particularly the moisture spikes that can be attributed to precipitation events.

Modeled subsurface temperature compares fairly well in both amplitude and timing with observations at SMOA at both 5 and 30 cm (Figure 2-12). There is a small time offset in the modeled temperatures at a depth of 30 cm (Figure 2-12b), but the overall match is fairly good (Figure 2-12c). At the same depths at SMMF (Figure 2-13), the modeled temperatures are reduced in amplitude and delayed in time when compared

to observations (red and green models in a and b, respectively). This time delay is strongly related to the effects of the snow cover that is modeled at SMMF. Since the modeled snow depth (Figure 2-9) is so great, the overall effect is to reduce the modeled ground temperatures. As seen at 30 cm depth, the result is strongly reduced amplitudes that exceeds 5 °C. Further, the timing related to the increase in temperatures after the snow melts is delayed in the model results. Great improvement is made when using the incoming solar radiation observations from SMOA. The resultant modeled ground temperatures (Figure 2-13, black and yellow lines) are much closer to the observed temperatures, although the modeled temperatures at 5 cm are generally warmer than the observations. The temperatures at 30 cm are well matched using this new input, showing the close tie between incoming solar radiation and ground temperature.

Discussion

Previous studies have investigated the effects of land cover changes, including deforestation and clear-cutting, on ground temperatures and subsurface hydrologic conditions [e.g., *Lewis and Wang*, 1998; *Lewis*, 1998; *Beltrami and Kellman*, 2003; *Iwahana et al.*, 2005; *Nitoui and Beltrami*, 2005; *Ferguson and Beltrami*, 2006; *Bense and Beltrami*, 2007; *Taggart et al.*, 2011]. *Lewis and Wang* [1998] report ground warming of 1 to 2 °C in Canadian boreholes where deforestation had occurred. They attribute the warming to the addition of heat into the ground that was previously utilized for transpiration in the forest. *Lewis* [1998] furthers this discussion with an analysis of the effects of deforestation on ground surface temperatures. Deforestation will warm the ground temperatures, introducing a warming bias in ground temperatures that is modeled

as a step change occurring at the time of deforestation [*Lewis*, 1998]. However, *Lewis* [1998] claims that as deforestation occurs, that air temperatures will increase in the deforested regions, matching ground temperatures. We do not observe this change, rather, ground temperatures respond to the changes in solar radiation.

Beltrami and Kellman [2003] show the results of two closely spaced stations in Nova Scotia, Canada. They report warmer ground temperatures in the spring and summer, similar to that observed in Oregon (Figure 2-7). Further, *Beltrami and Kellman* [2003] observe the importance of solar radiation to the ground temperatures at the field site in their study, but, in contrast to this study, do not find that solar radiation is as important in the forested site.

Iwahana et al. [2005] show that, at their paired sites in a permafrost region of Siberia, an increase in soil temperature occurs in the first year after land cover change after which no further change in soil temperature occurs. It is not clear if the vegetation at their cleared site is returning, as we observed at our clear-cut site. If so, we would expect that ground temperatures would cool. *Iwahana et al.* [2005] also report an increase in soil water content at the cleared site that they ascribe to the decrease in evapotranspiration from the loss of the forest. Unfortunately, we do not have data immediately after clear cutting to know if this is occurring at our sites; however, we do not observe changes in the soil moisture differences over time as the forest regrows at our open site that would indicate initially changed conditions (Figure 2-7).

Several papers [*Nitoiu and Beltrami*, 2005; *Ferguson and Beltrami*, 2006; and *Bense and Beltrami*, 2007] investigate through modeling how deforestation can perturb ground temperatures spatially away from the land cover change. Deforestation would

increase the amount of energy received at the ground surface, thus warming the borehole temperatures. *Nitoiu and Beltrami* [2005] noted that as the forest regrows, the conditions will return to those that were preexisting, but the bias in temperature would remain. A major assumption in their model [*Nitoiu and Beltrami*, 2005] was that regrowth would require times on the order of 100 years. However, at our site, we see significant regrowth and a return to background conditions in only a few years. While a bias in the borehole temperatures would be introduced by deforestation, at our site, it would not be as significant as the modeling by *Nitoiu and Beltrami* [2005] would suggest. The other two studies [*Ferguson and Beltrami*, 2006; *Bense and Beltrami*, 2007] both model deep borehole temperatures and lateral flow conditions. Our study investigated subsurface conditions in the upper meter and did not observe conditions such as modeled by these studies.

Lastly, *Taggart et al.* [2011] investigated the effects that shading has on carbon storage in soils and found that shading of soils and regrowth of vegetation in a peatland in North Carolina increased the storage of carbon in the soil. While we did not measure carbon storage, the regrowth of our open site holds the potential for increased storage of carbon.

Conclusions

Five years of observations at the Soapgrass Mountain site in the Oregon Cascades permit the following conclusions:

1. Subsurface temperatures generally follow the patterns of air temperature. However, subsurface temperatures are largely influenced by incoming solar radiation, as

is observed by the decreasing ground temperatures in the open area from 8.3 °C to 7.8 °C (litter temperatures). Over this time period, the air temperatures in the open area actually increase from 7.7 to 8.3 °C, while incoming radiation decreases from 304 to 240 μmol m^{-2} sec^{-1}. This decrease corresponds to vegetation regrowth and shading of the ground in the open area.

2. The exception to the air temperature and solar radiation influence on the ground temperature is during the winter when there is snow cover. This provides for differences that we observe between the open area and the mature forest in the spring, where snow cover remains on the ground longer in the mature forest between one to two weeks. This occurs even though the amount of snow on the ground in the mature forest is generally less than half the depth of the open area snow throughout the winter.

3. Precipitation has the greatest impact on soil moisture. Changes in soil moisture can be directly correlated to precipitation events. However, there is no apparent change in subsurface temperatures related to precipitation. Also, despite the vegetation differences, precipitation differences at the surface over the course of a year are small, with the open area receiving an average of less than 2 mm day^{-1} more than the mature forest over the course of the year, despite large differences for individual events averaging up to 50 mm day^{-1}. Thus, over the course of our observations, there are small differences in soil moisture between the open area and mature forest sites between 5.6 and 14.6%.

4. Land surface modeling of the sites only works if the open area radiation values are used – otherwise, the snow cover is too deep (exceeding 10 m!) and lasts too long into

the summer. This greatly influences the subsurface temperatures as the snow cover insulates the ground from the air temperatures.

References

Barlage, M., Chen, F., Tewari, M., Ikeda, K., Gochis, D., Dudhia, J.,Rasmussen, R., Livneh, B., Ek, M., and Mitchell, K., 2010. Noah land surface model modifications to improve snowpack prediction in the Colorado Rocky Mountains. J. Geophys. Res. 115, D22101, doi:10.1029/2009JD013470.

Bartlett, M. G., Chapman, D.S., and Harris, R.N., 2004. Snow and the ground temperature record of climate change. J. Geophys. Res. 109, F04008, doi:10.1029/2004JF000224.

Bartlett, M. G Chapman, D.S., and Harris, R.N., 2005. Snow effect on North American ground temperatures, 1950–2002. J. Geophys. Res. 110, F03008, doi:10.1029/2005JF000293.

Beedlow, P.A., Tingey, D.T., Lee, E.H., Phillips, D.L., Andersen, C.P., Waschmann, R.S., and Johnson, M.J., 2007. Sapwood moisture in Douglas-fir boles and seasonal changes in soil water. Can. J. For. Res. 37, 1263–1271, doi:10.1139/X06-319.

Beltrami, H., 2002. Climate from borehole data: Energy fluxes and temperature since 1500. Geophys. Res. Lett. 29(23), 2111, doi:10.1029/2002GL015702.

Beltrami, H., and Kellman, L., 2003. An examination of short- and long-term air-ground temperature coupling. Global Planet. Change. 38, 291-303.

Bense, V., and Beltrami, H., 2007. Impact of horizontal groundwater flow and localized deforestation on the development of shallow temperature anomalies. J. Geophys. Res. 112, F04015, doi:10.1029/2006JF000703.

Bierlmaier, F. A., and McKee, A., 1989. Climatic summaries and documentation for the Primary Meterological Station, H. J. Andrews Experimental Forest, 1972 to 1984. USDA Forest Service, Pacific Northwest Research Station, Portland, OR.

Bradley, R. S., 1999. Paleoclimatology: Reconstructing climates of the Quaternary, second ed. Academic Press, San Diego, California.

Carslaw, H.S., and Jaeger, J.C., 1959. Conduction of Heat in Solids, second ed. Oxford University Press, London.

Chen, F., Mitchell, K.E., Schaake, J., Xue, Y., Pan, H.-L., Koren, V., Duan, Q.Y., Ek, M., and Betts, A., 1996. Modeling of land-surface evaporation by four schemes and comparison with FIFE observations. J. Geophys. Res. 101, 7251–7268.

Chen, F., and Dudhia, J., 2001a. Coupling an advanced land-surface/hydrology model with the Penn State/NCAR MM5 modeling system. Part I: Model description and implementation. Mon. Wea. Rev.. 129, 569–585.

Chen, F., and Dudhia, J., 2001b. Coupling an advanced land-surface/hydrology model with the Penn State/NCAR MM5 modeling system. Part II: Model validation. Mon. Wea. Rev. 129, 587–604.

Dudhia, J., 1993. A nonhydrostatic version of the Penn State/NCAR mesoscale model: Validation tests and simulations of an Atlantic cyclone and cold front. Mon. Wea. Rev. 121, 1493–1513.

Ek, M. B., Mitchell, K.E., Lin, Y., Rogers, E., Grunmann, P., Koren, V., Gayno, G., and Tarpley, J.D., 2003. Implementation of Noah land surface model advances in the National Centers for Environmental Prediction operational mesoscale Eta model. J. Geophys. Res. 108(D22), 8851, doi:10.1029/2002JD003296.

Evans, J. P., Oglesby, R.J., and Lapenta, W.M., 2005. Time series analysis of regional model climate performance. J. Geophys. Res. 110, D04104, doi:10.1029/2004JD005046.

Ferguson, G., and Beltrami, H., 2006. Transient lateral heat flow due to land-use changes. Earth Planet. Sci. Lett. 242, 217-222.

Gutman, G. and Ignatov, A., 1998. The derivation of the green vegetation fraction from NOAA/AVHRR for use in numerical weather prediction models. Int. J. Remote Sens. 19, 1533-1543.

Hogue, T. S., Bastidas, L.A., Gupta, H.V., Sorooshian, S., Mitchell, K., and Emmerich, W., 2005. Evaluation and transferability of the Noah land surface model in semiarid environments. J. Hydrometeor. 6, 68–84.

Idso, S.B., and Jackson, R.D., 1969. Thermal radiation from the atmosphere. J. Geophys. Res. 74, 5397-5403.

Iwahana, G., Machimura, T., Kobayashi, Y., Federov, A.N., Konstantinov, P.Y., and Fukuda, M., 2005. Influence of forest clear-cutting on the thermal and hydrological regime of the active layer near Yakutsk, eastern Siberia. J. Geophys. Res. 110, G02004, doi:10.1029/2005JG000039.

Lachenbruch, A.H., and Marshall, B.V., 1986. Changing climate: Geothermal evidence from permafrost in the Alaskan Arctic. Science. 234, 689-696.

Lewis, T., and Wang, K., 1998. Geothermal evidence of deforestation-induced warming: implications for the climatic impact of land development. Geophys. Res. Lett. 25, 535-538.

Lewis, T., 1998. The effect of deforestation on ground surface temperatures. Global Planet. Change. 18, 1-13.

Lin, X., Smerdon, J.E., England, A.W., and Pollack, H.N., 2003. A model study of the effects of climatic precipitation changes on ground temperatures. J. Geophys. Res. 108(D7), 4230, doi:10.1029/2002JD002878.

Marht, L., and Pan, H.-L., 1984. A two-layer model of soil hydrology. Boundary Layer Meteorol. 29, 1-20.

Mote, P.W., Hamlet, A.F., Clark, M.P., and Lettenmaier, D.P., 2005. Declining mountain snowpack in western North America. Bull. Amer. Meteor. Soc. 86, 39–49.

National Research Council, 2006. Surface temperature reconstructions for the last 2,000 years. The National Academies Press.

Nitoiu, D., and Beltrami, H., 2005. Subsurface thermal effects of land use changes. J. Geophys. Res. 110, F01005, doi:10.1029/2004JF000151.

Pan, H.-L., and Mahrt, L., 1987. Interaction between soil hydrology and boundary-layer development. Boundary Layer Meteorol. 38, 185-202.

Pollack, H. N., Smerdon, J.E., and van Keken, P.E., 2005. Variable seasonal coupling between air and ground temperatures: A simple representation in terms of subsurface thermal diffusivity. Geophys. Res. Lett. 32, L15405, doi:10.1029/2005GL023869.

Putnam, S.N., and Chapman, D.S., 1996. A geothermal climate change observatory: First year results from Emigrant Pass in northwest Utah. J. Geophys. Res. 101, 21877-21890.

Radell, D.B., and Rowe, C.M., 2008. An Observational Analysis and Evaluation of Land Surface Model Accuracy in the Nebraska Sand Hills. J. Hydrometeor. 9, 601-621.

Rao, C.R.N., 1984. Photosynthetically active components of global solar radiation: measurements and model computations. Arch. Met. Geoph. Bioclim. Ser. B 34, 353-364.

Robinson, D.A., and Kukla, G., 1985. Maximum surface albedo of seasonally snow-covered lands in the Northern Hemisphere. J. Climate Appl. Meteor. 23, 1626-1634.

Sheffield, J., et al., 2003. Snow process modeling in the North American Land Data Assimilation System (NLDAS): 1. Evaluation of model simulated snow cover extent. J. Geophys. Res. 108(D22), 8849, doi:10.1029/2002JD003274.

Skamarock, W. C., Klemp, J.B., Dudhia, J., Gill, D.O., Barker, D.M., Wang, W., and Powers, J.G., 2005. A description of the Advanced Research WRF version 2. NCAR Tech Note NCAR/TN-468+STR.

Skamarock, W. C., Klemp, J.B., Dudhia, J., Gill, D.O., Barker, D.M., Duda, M., Huang, X.-Y., Wang, W., and Powers, J.G., 2008. A description of the Advanced Research WRF version 3. NCAR Tech Note NCAR/TN-475+STR.

Smerdon, J. E., Pollack, H.N., Enz, J.W., and Lewis M.J., 2003. Conduction-dominated heat transport of the annual temperature signal in soil. J. Geophys. Res. 108(B9), 2431, doi:10.1029/2002JB002351.

Shrestha, R., and Houser, P., 2010. A heterogeneous land surface model initialization study. J. Geophys. Res. 115, D19111, doi:10.1029/2009JD013252.

Stoelinga, M.T., Albright, M.D., and Mass, C.F., 2010. A New Look at Snowpack Trends in the Cascade Mountains. J. Clim. 23, 2473-2491.

Taggert, M.J., Heitman, J.L., Vepraskas, M.J., and Burchell, M.R., 2011. Surface shading effects on soil C loss in a temperate muck soil. Geoderma. 163, 238-246.

Turcotte, D.L., and Schubert, G., 2002. Geodynamics, second ed. Cambridge University Press, New York.

Udo, S.O., and Aro, T.O., 1999. Global PAR related to global solar radiation for central Nigeria. Agric. For. Meteorol. 97, 21-31.

Yang, Z.-L., Dickinson, R.E., Henderson-Sellers, A., and Pitman, A.J., 1995. Preliminary study of spin-up processes in land surface models with the first stage data of Project for Intercomparison of Land Surface Parameterization Schemes Phase 1(a). J. Geophys. Res. 100, 16,553–16,578, doi:10.1029/95JD01076.

Zhang, T., 2005. Influence of the seasonal snow cover on the ground thermal regime: An overview. Rev. Geophys. 43, RG4002, doi:10.1029/2004RG000157.

CHAPTER 3

A WEB-BASED RESOURCE FOR INVESTIGATING ENVIRONMENTAL CHANGE: THE EMIGRANT PASS OBSERVATORY

Abstract

We present a user-friendly, data-driven website (http://thermal.gg.utah.edu/facilities/epo/) for a geothermal, climate-change observatory that is educational for the general public, students, and researchers alike. The Emigrant Pass Observatory (EPO), located in the Grouse Creek Mountains in northwestern Utah, gathers both meteorological data (solar radiation, air temperature, rainfall, wind speed and direction, and snow depth) and subsurface temperatures in shallow drillholes. Our website has three main functions: 1) it provides a tutorial for understanding both local climate and climate change, and their relation to diffusion of temperatures into the Earth's subsurface, 2) it facilitates user-defined accessibility to download available climate data, and 3) it contains lesson ideas for using real data to understand local climate. EPO data and resources are ideal for active learning projects. Additionally, our collaboration with ongoing outreach projects (e.g., GK-12) in Utah promote the use and understanding of

climate change data among students and educators, thus filling a valuable niche in local education.

Introduction

The surface temperature of our planet has increased on average by nearly one degree Celsius over the last century, with much of the warming occurring since 1975 [*Hansen et al.*, 2010, *Brohan et al.*, 2006, *Smith and Reynolds*, 2005]. The fourth, and most recent, assessment of the Intergovernmental Panel on Climate Change [*IPCC*, 2007] showed that the only way to explain the temperature increase is via anthropogenic causes. Although there is still lingering "debate" among the public and policymakers over the cause of climate change [e.g., *Newell and Pitman*, 2010], when past and future temperature change is put into perspective [*Chapman and Davis*, 2010], there can remain little doubt about its anthropogenic origin.

As *Newell and Pitman* [2010] point out, part of the uncertainty among non-scientists over the reality of global warming has psychological underpinnings related to how people make decisions. An additional contribution to this uncertainty can be traced to deficiencies in science education as has been reported on by several studies authored by scientific [*American Association for the Advancement of Science*, 1990; *National Research Council*, 2011] and government [*National Science Foundation*, 1996] bodies. A key issue in all of these studies is that "hands-on" or active learning is an important aspect of science literacy. Using and analyzing real data is one way of providing students with an active learning environment [e.g., *Hays et al.*, 2000].

This commentary follows an assertion by *Martin and Howell* [2001] that science should be "minds on." According to *Martin and Howell* [2001], "minds on" science involves a student's exploration of a scientific question as opposed to focusing on the answer. This investigation of the question requires students "*to analyze large sets of real data, to evaluate the data critically, to observe patterns and anomalies, to make inferences and predictions based on the data, to interpret the data, and to form testable hypotheses to explain their observations*" [*Martin and Howell*, 2001, 158].

To be able to accomplish "minds on" project learning, it is necessary to have access to both the relevant tools and datasets required to satisfy the project objectives [*Roberts et al.*, 2010]. The use of such tools in science education is becoming more commonplace throughout the educational system [*Underwood et al.*, 2008], and online data use in the classroom has been shown to enhance student satisfaction and learning [*Brey*, 2000]. One of the key issues is knowing where to find such data.

The Emigrant Pass Observatory (EPO; http://thermal.gg.utah.edu/facilities/epo/) provides a way of understanding how climate change is studied and offers real research data that can be obtained easily through an online interface. This commentary describes the operations of the EPO, the data products that are available, and potential lesson ideas that can be used by interested educators for students in learning about climate processes and change.

Emigrant Pass Observatory

The Emigrant Pass Observatory (EPO) is located at the southern end of the Grouse Creek Mountains of northwestern Utah (Figure 3-1). It was established in 1993

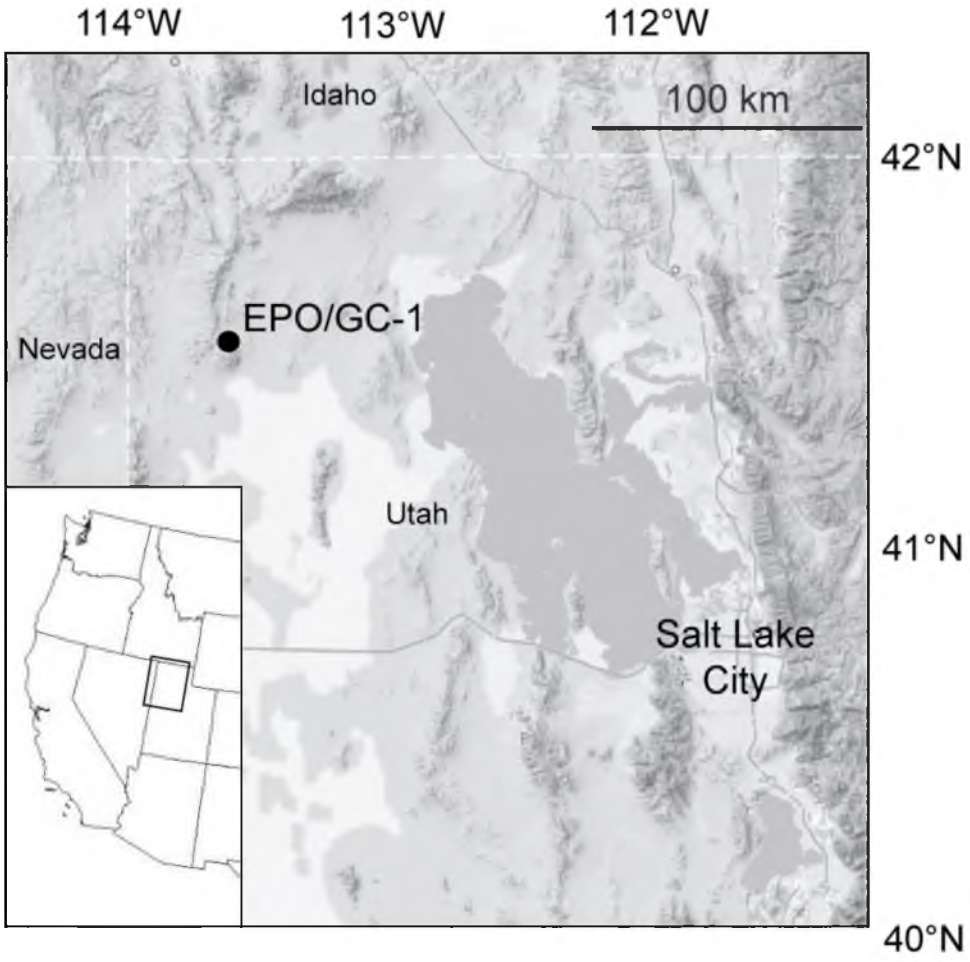

Figure 3-1. Map of northwestern Utah, USA, showing the Emigrant Pass Observatory (modified from *Davis et al.*, 2010).

next to a 150 m deep borehole GC-1 as part of a climate change observatory that would allow concurrent monitoring of both meteorological conditions (such as air temperature, solar radiation, snow, and rainfall) and subsurface temperatures [*Putnam and Chapman*, 1996]. The station ran continually through 2004, with minor operational setbacks due to battery, data storage, and instrument failures [*Bartlett et al.*, 2006]. A major upgrade of the station near the end of 2004 allowed telemetry of daily observations at EPO [*Bartlett et al.*, 2006], and near 100 percent data recovery.

The borehole and weather station are located on a granitic outcrop in the midst of a sparsely vegetated area of piñon pine and juniper (Figure 3-2). The topography is generally flat with a gentle slope to the northeast. These factors aid in making this desert environment an ideal location for such an observatory.

The instruments at EPO include a solar powered Campbell Scientific CR-10 data logger that controls a collection of meteorological instruments (air temperature, solar radiation, precipitation, snow depth, wind speed, and wind direction) and several shallow thermistor strings designed to measure temperature in the granite outcrop and nearby soil (Figure 3-2). The data logger interrogates the sensors every 60 seconds and stores 30-minute averages.

Use of EPO and Boreholes to Study Climate

Boreholes, long used to investigate heat flowing out of the Earth through measurements of temperature with depth, are also an important source of information of changing temperatures at the surface of the earth. Changing surface temperatures diffuse into the subsurface, as described by the one-dimensional heat diffusion equation,

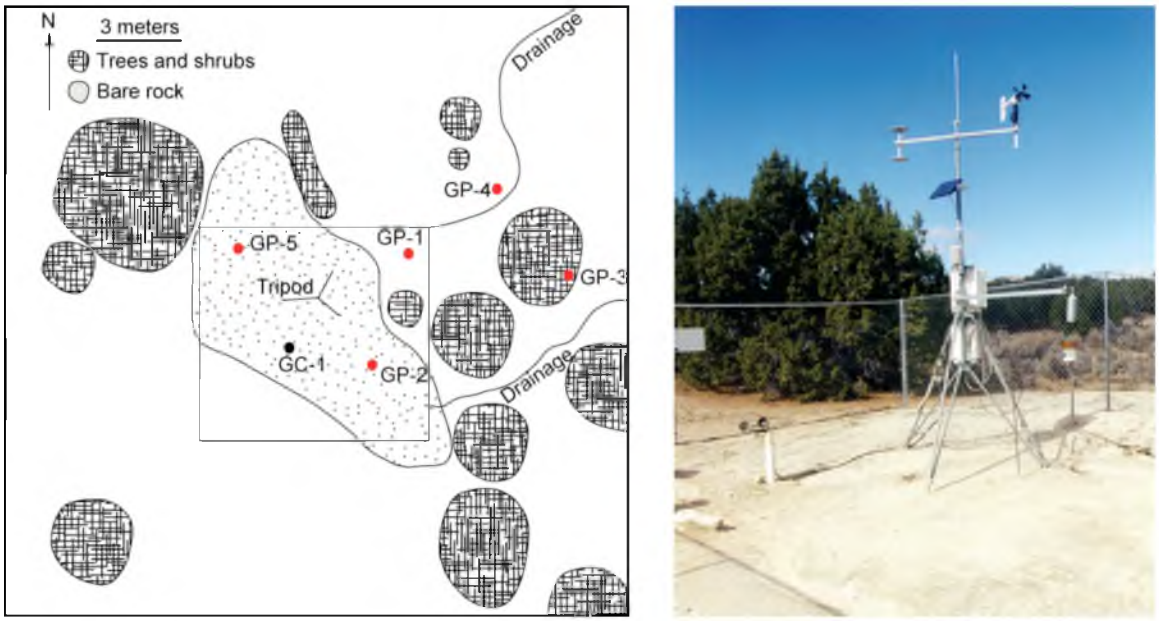

Figure 3-2. The Emigrant Pass geothermal climate change observatory EPO. (Left) Cartoon map view of EPO with locations of the ground temperature probes (GP1-5), the borehole GC-1, and surrounding vegetation. (Right) Image of EPO looking towards the large piñon pine on the northwest of the enclosure.

$$\frac{\partial T(z,t)}{\partial t} = \alpha \frac{\partial^2 T(z,t)}{\partial z^2}, \qquad (3\text{-}1)$$

where T is temperature, z is depth, t is time, and α is thermal diffusivity. Because it is a diffusive process, there is both an attenuation of the temperature amplitude and a phase lag (Figure 3-3) in the ground temperatures. Figure 3-3 shows a simplified annual sinusoidal surface temperature wave (Figure 3-3, solid line z = 0 m) with a mean temperature of ~10°C and an amplitude of 20°C. At a depth of 1 m (Figure 3-3, dashed line), the amplitude of the temperature wave is 73% of the surface amplitude, and the peaks and troughs occur 18 days later than at the surface. At a depth of 5 m (Figure 3-3, dotted line), the amplitude is further attenuated to 41% of the surface amplitude, and the peak occurs 91 days after the surface peak. Also noteworthy in this simplified model, the surface temperature is below freezing for 121 days, whereas at 1 m, the temperature is below freezing for only 94 days. The ground at 5 m depth never freezes, with a minimum temperature of 5.9°C. This attenuation property allows one to avoid freezing water pipes by burying the pipes to a particular depth.

The process of diffusing surface temperature into the subsurface can be used to examine changing surface air temperature (SAT) over periods of years, decades, and centuries. Changes in SAT (and hence surface ground temperatures) produce transient departures from the background, steady-state thermal regime measured in boreholes. Figure 3-4 illustrates a hypothetical, fluctuating SAT plotted with the mean as zero (Figure 3-4a). Beginning in 1900, this imaginary SAT has a warming trend of nearly 20 years before slowly cooling for the next 40 years. Following this overall cooling trend is approximately 40 years of warming until the record ends in 2000. If one were to measure

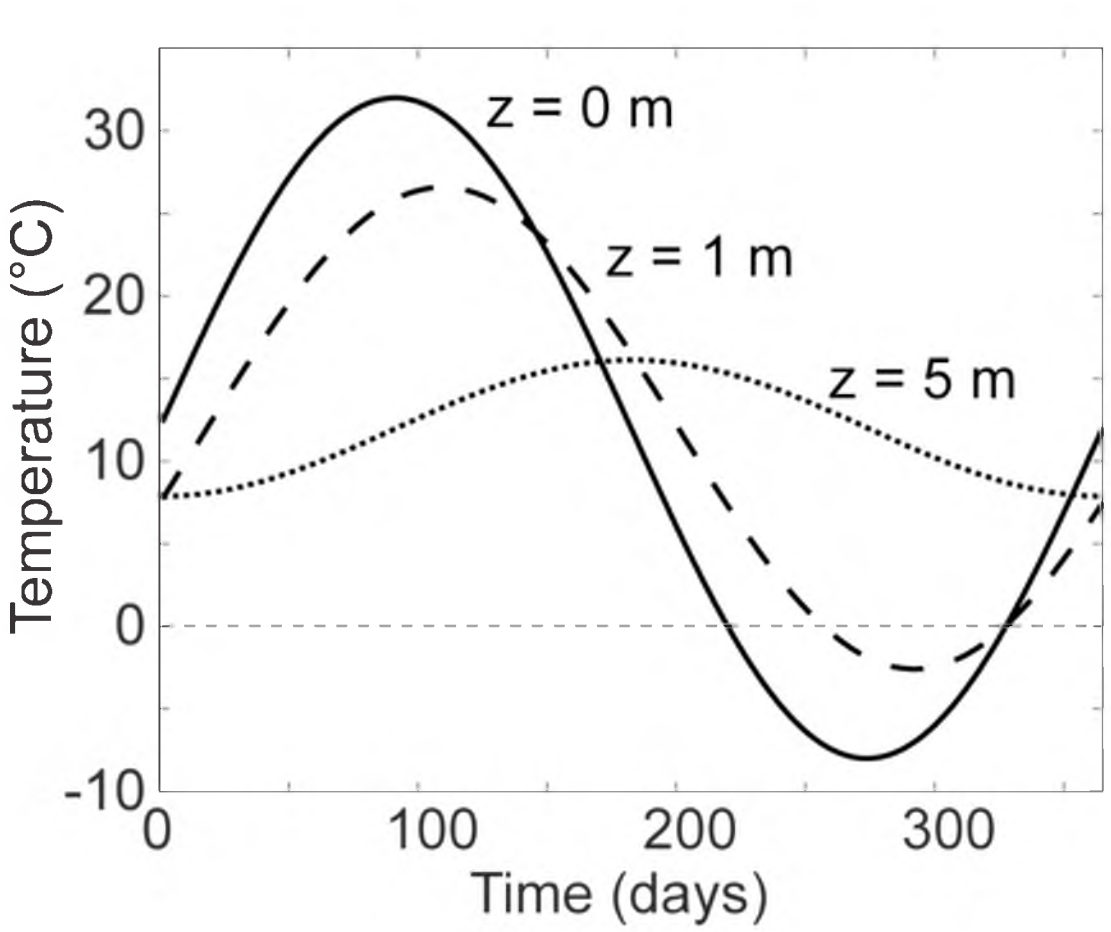

Figure 3-3. Diffusion of a sinusoidal annual surface temperature wave into the subsurface. Note the phase lag and attenuation of the surface temperature. See text for details.

the ground temperatures in a borehole at three distinct times (1956, 1976, and 1998; indicated by triangles, Figure 3-4a), the resulting borehole temperature-depth profiles would be affected by the fluctuating SAT. In the absence of a changing surface temperature, the constant, background thermal gradient (Figure 3-4b, heavy solid line) facilitates heat flowing steadily out of the Earth and would be drawn to show the surface temperature intercept equal to the mean surface temperature. However, as the SAT changes (remembering that in this case, it warms, cools, and warms again), a transient temperature anomaly is recorded in the subsurface temperature measurements that are different from the background thermal profile (Figure 3-4b). In our example, the initial borehole temperature measurements are made in 1956. The resultant temperature-depth profile (Figure 3-4b, dotted line) is cooler than the background thermal gradient to a depth of approximately 50 m, due to the borehole temperatures being measured after nearly 40 years of SAT cooling. Returning to the borehole after 20 years, measured ground temperatures show that the anomaly from the cool temperatures has continued to diffuse into the subsurface, with temperatures cooler than the background geotherm extending to around 75 m (Figure 3-4b, thin solid line). However, the SAT has begun warming during this 20-year period, so the upper portion of the borehole is now warming, with the uppermost temperatures being greater than the background thermal profile (Figure 3-4b, thin solid line). With continued warming over the next two decades, a final borehole temperature-depth profile would show the transient anomaly to be warmer than the background temperature-depth profile (Figure 3-4b, dash-dot line) down to a depth of about 45 m. Below this depth, the earlier cooling trend measured previously still affects the borehole temperatures, as temperatures below 50 m are slightly cooler than

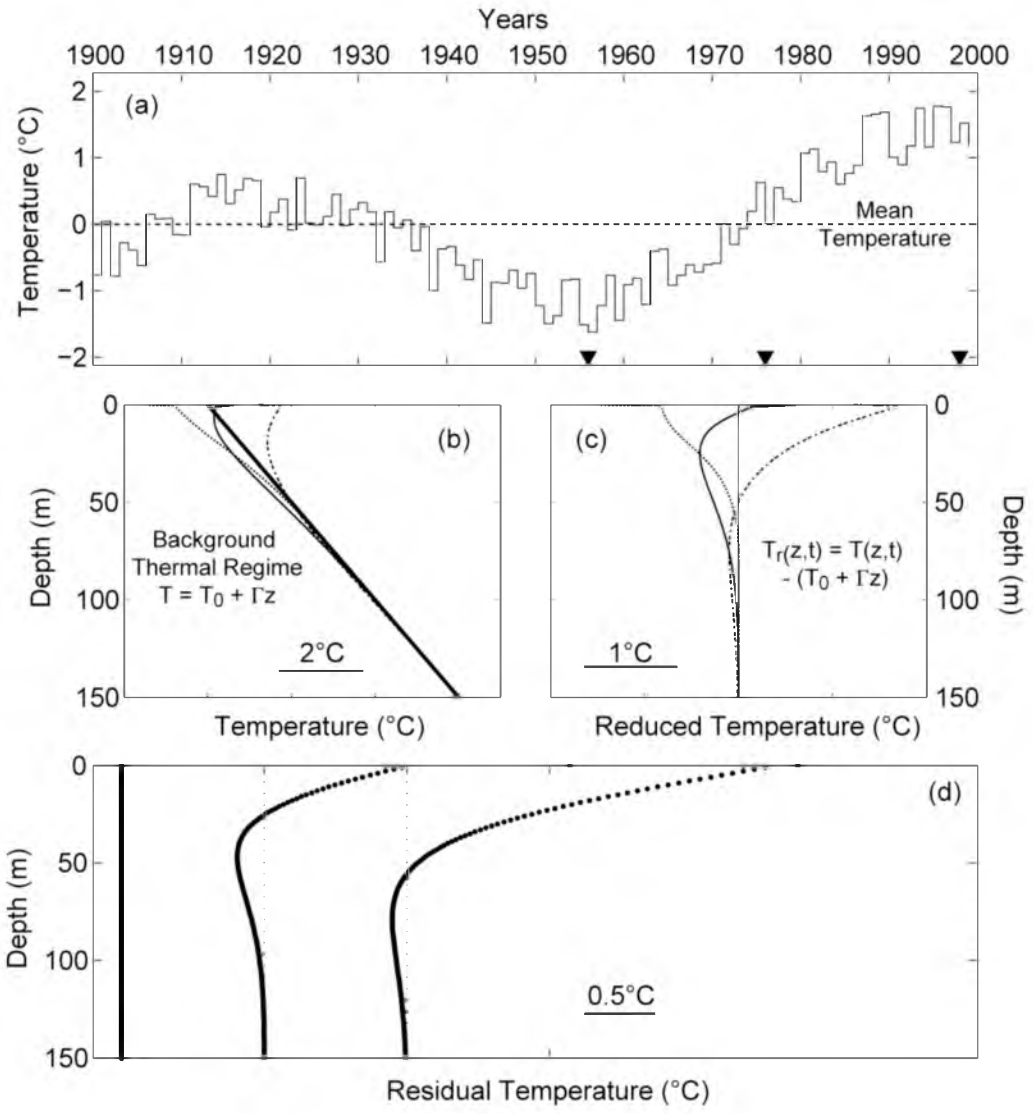

Figure 3-4. Basic aspects of using borehole temperatures to understand surface temperature change. (a) A 100-year record of SAT plotted with the mean temperature as zero. Borehole temperatures are measured at three distinct times as indicated by triangles. (b) Temperature-depth profiles at these three times shown with respect to the background thermal gradient (solid line). (c) Reduced temperature profiles with the background thermal gradient removed. (d) Temperature differences with respect to the initial temperature log. Figure modified from *Davis et al.* [2011].

background. These cooler temperatures extend to below 100 m depth, although they are strongly reduced due to the diffusive nature of this process as described by Equation 3-1.

Because the transient temperature component is often small (the cool temperatures extending to below 100 m in the third temperature-depth profile, for example), it is convenient to remove the background thermal gradient and present the transient anomaly as reduced temperature (Figure 3-4c) with an expanded temperature scale. This transform allows one to isolate the transient anomaly and make comparisons with the steady-state case. In our example, the effects of cooling extend the entire depth of the borehole by the final borehole temperature log (Figure 3-4c, dash-dot line). In practice, instrument precision and geologic noise limit detection of small signals and it would be difficult to see the entire anomaly. However, the larger the anomaly, the deeper it can be identified, such that surface temperature reconstructions for the past 100 years can be found in the upper 150 m of the Earth, and surface temperature change in the past millennium can be made from temperatures measured in 500 m deep boreholes (for further information see *Davis et al.* [2011] and references therein).

When multiple borehole temperature-depth profiles are available, it is most informative to examine the temperature changes between logs by differencing them relative to the initial log (Figure 3-4d). Differencing allows one to identify transient temperatures and eliminate perturbations in a temperature profile not related to climate. A convincing case for climate reconstruction can be made when air temperature changes are modeled and produce good fits to the changes seen in the differenced temperature. For further information, see *Davis et al.* [2010].

Monitoring of meteorological variables, in addition to temperature, are important to understanding coupling between ground and air temperatures. Snow, for example, insulates the ground from the very cold conditions in the air, resulting in the ground being warmer than would be expected. On the other hand, site conditions like excessive vegetation or shade, in association with incoming solar irradiance, can result in cooler ground temperatures. A site such as EPO where changing conditions are continually monitored allows us to connect ground and air temperatures, particularly in an effort to investigate past climate changes.

Data Products

The Emigrant Pass Observatory web site (http://thermal.gg.utah.edu/facilities/epo/) allows specific downloading of climate parameters measured at the site. Individual sensors and time periods can be selected for downloading (Table 3-1). With simple text files as output, the web site allows for easy use in data analysis packages such as Matlab or Microsoft Excel (Figure 3-5). For example, Figure 3-5 shows meteorological variables and ground temperature measured at EPO during one annual cycle starting in January 2007. The surface air temperature (SAT) (Figure 3-5a) clearly shows the seasonal variation but also fluctuates with shorter periods indicating cold and hot spells. Air temperature at the EPO site in Utah varies by 50°C during the year, from a low of -15 to a maximum of 35°C. Ground temperatures can be seen to follow the SAT, with similar patterns of temperature change throughout the year, especially for the shallow measurements, but are warmer than air temperatures in the summer months. The attenuation and the phase lag of the ground temperatures that are described by Equation 1

Table 3-1. Available sensors at EPO (modified from *Bartlett et al.*, 2006).

Measured[1] parameter	Precision[2]	Installation[3]
Air temperature	0.05 K	2 m above granite
Solar radiation	0.1 Wm^{-2}	Incident
Rainfall	0.1 mm	1-m mast height
Snow Depth	1.0 mm	Sonar "pinger"
Wind Speed	0.04 m s^{-1}	3-m mast height
Wind Direction	5.0°	3-m mast height
Wind Variability	5.0°	3-m mast height
Ground Temperature	0.01 K	0.025, 0.1, 0.2, 0.5, 1.0 m

[1] Meteorological variable measured at EPO.
[2] Precision of individual instruments and data at EPO.
[3] Location (height or depth) of instruments at EPO.

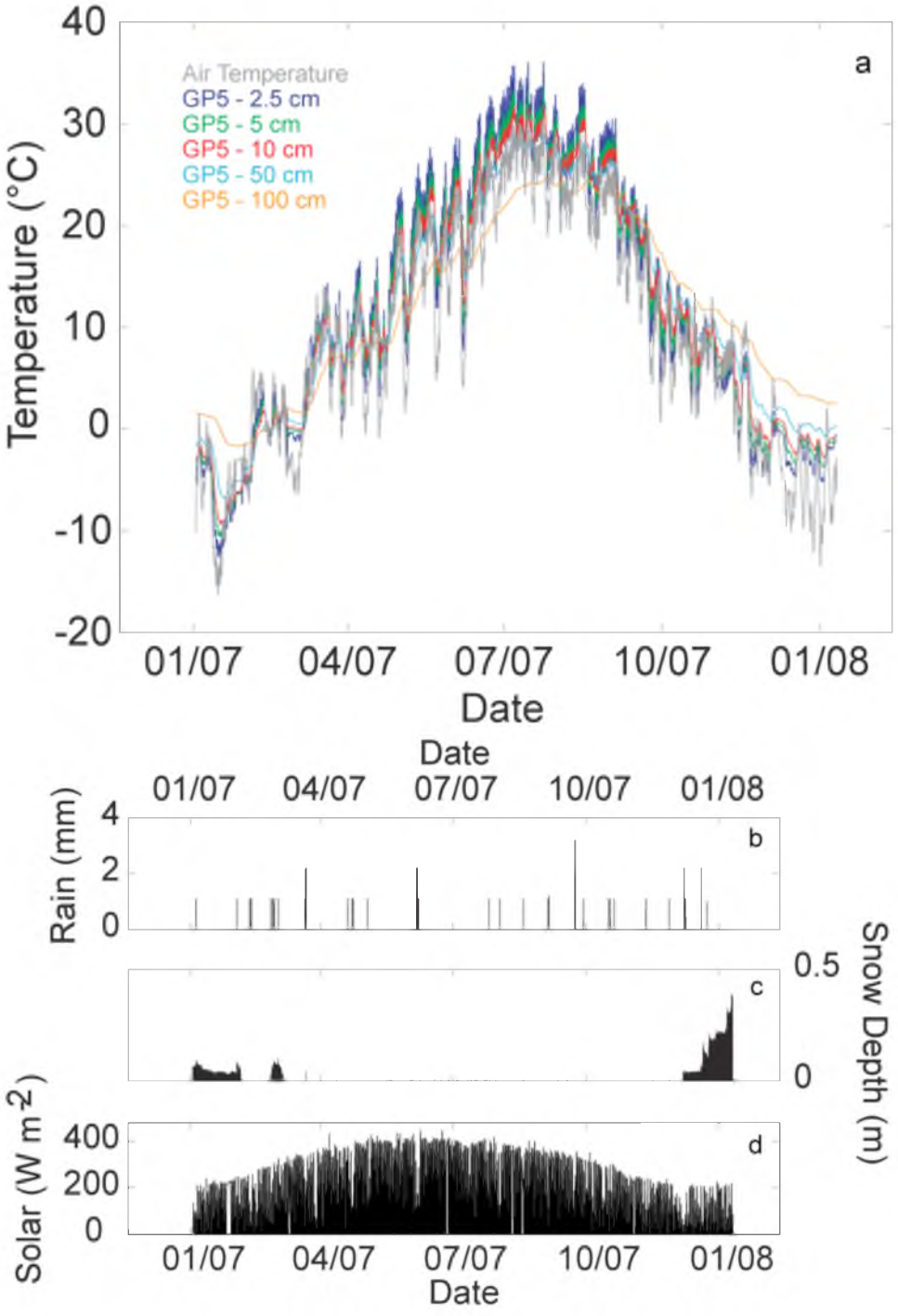

Figure 3-5. Meteorological variables and ground temperatures at EPO for the year 2007. a) Daily air and ground temperatures. Note the tracking of air temperature by the ground temperature. b) Annual rainfall (75 mm). c) Snow depth. The 2007 - 2008 winter was an exceptional snow year. d) Solar insolation.

are more apparent in the deeper measurements. The amplitude of the temperature fluctuation at 1 m is greatly subdued not only annually, but high-frequency variation is not seen at shorter time scales. There is also a notable lag in the time of peak SAT and peak ground temperature at 1 m.

Other available data include precipitation in the form of both rain (Figure 3-5b) and snow (Figure 3-5c), as well as solar insolation (Figure 3-5d). Precipitation at EPO is very low, with small rain events throughout the year (Figure 3-5b). The majority of the precipitation comes in the form of snow, with some years having little snow (e.g., 2006 – 2007) and others having considerably more (e.g., 2007 – 2008; Figure 3-5c). Solar radiation at the site varies throughout the year (Figure 3-5d) and is the primary driver of temperatures recorded at EPO [*Putnam and Chapman*, 1996; *Bartlett et al.*, 2006].

A closer examination of the SAT and the ground temperatures is shown in Figure 3-6. Over the course of one week, the SAT has a daily variation of greater than 10°C and is highly variable throughout the day. The shallowest ground temperature at 2.5 cm depth follows the general trend seen in the SAT, but with an obvious time lag. The ground temperature at 2.5 cm also is much warmer at its peak than the SAT. This observation can be directly related to the heating the granite surface at EPO receives from the incoming solar radiation [*Putnam and Chapman*, 1996]. Also notable is the attenuation of the ground temperatures with depth when compared with the SAT (Figure 3-6).

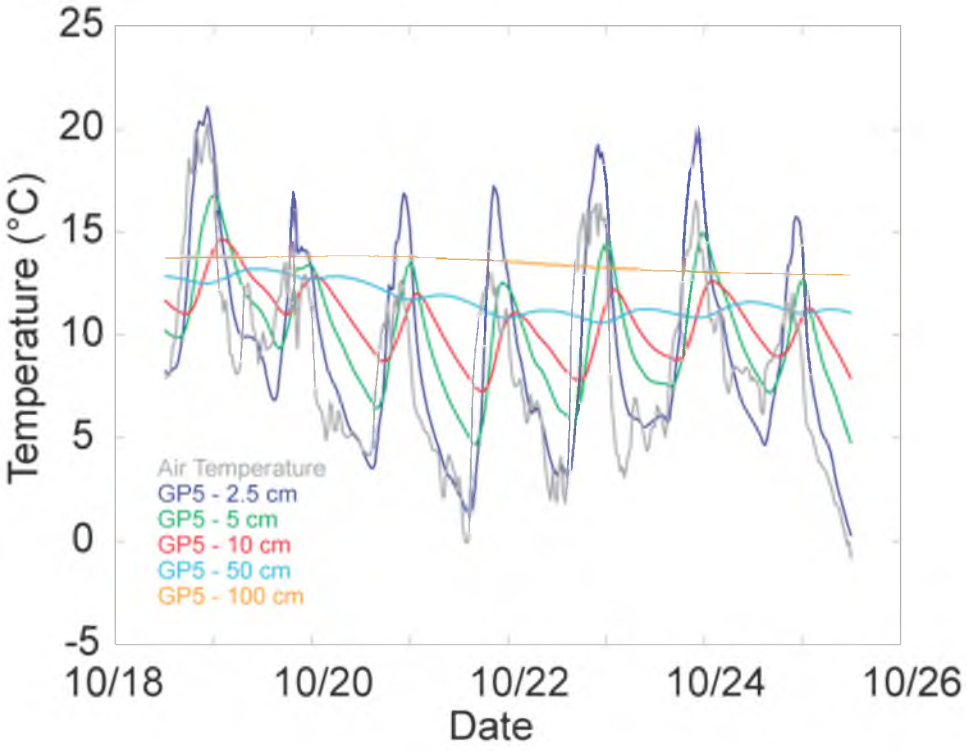

Figure 3-6. Air and ground temperatures at EPO over the course of one week in October of 2009. The phase lag and attenuation of the air temperature is clearly seen in the subsurface temperatures.

Lesson Ideas

Depending on the grade level of the students (K-12, undergraduate, graduate), as well as the objective of the lesson or class, it may be necessary to introduce some basic principles (e.g., how the sun affects climate) prior to using the EPO data. However, it may also be useful to just "jump in" and begin examining the data. For many students, seeing and using real scientific data can lead to greater interest [*Brey*, 2000], so the "jump in" approach can be effective. Alternatively, we suggest performing a pretest that examines a student's prior knowledge and understanding. This can be an excellent springboard on the direction to proceed [e.g., *Martin and Howell*, 2001]. In such a pre-test, students can first be asked to sketch a plot of how air temperature changes over a given period of time. A good starting point is looking at the daily variation of temperature, as most students should be able to identify roughly the rise and fall of temperature that occurs over the course of a day. After discussing the student responses, a consideration and discussion of measured EPO air temperature is warranted. For example, the air temperature plotted in Figure 3-6 illustrates the warming of the air through the day, followed by cooling into the evening and night. However, the warming and cooling of the air temperature does not smoothly increase and decrease, but instead shows higher frequency fluctuations throughout the day. Inspection of other parameters such as solar radiation, wind, and precipitation could then elucidate what may be happening to cause the uneven rise and fall of air temperature. Is there a storm passing? Is it cloud cover? Examining this phenomenon gives students the "minds on" experience of working with and analyzing real-world data.

A second lesson could involve investigating how the ground temperatures change over time (Figure 3-6). A pretest procedure that asks students to sketch how ground temperatures would change with respect to air temperature might lead to a discussion on how hot the ground gets (e.g., a comparison of asphalt versus grass) and why this occurs (albedo effects). After this discussion, an examination of the ground temperatures would yield "minds on" questions such as why does the ground temperature change lag the air temperature change and why the ground temperatures have smooth variations with time. Further inquiry of the ground temperature data during and after the winter snow and an observation that ground cleared of snow freezes "hard" while ground covered by snow rarely freezes can also lead to excellent discussion and opportunities for inquiry-based learning.

In both cases discussed, data from EPO serve as a basis for understanding how changes at the surface affect the ground beneath our feet. This consideration provides an additional element for understanding climate and environmental change, as much climate-related data are limited to surface meteorological data only.

Outreach

The rich resource of climate information from the northwestern Utah EPO creates a potential for science outreach. One way we are promoting the use of our web site is with ongoing National Science Foundation sponsored GK-12 outreach projects in Utah. These projects promote the use of scientific data in the classroom through inquiry-based learning by placing University of Utah science graduate students in contact with elementary, middle, and high school students and educators in the Salt Lake City School

District. Through weekly meetings, graduate students are introduced to the EPO website and the various learning activities that are available. After presenting lessons in K-12 classrooms, these graduate students provide feedback and assessment that will help to improve the offerings of the website.

Summary

The Emigrant Pass Observatory in northwest Utah offers near-real time climate data that can easily be accessed for "minds on," inquiry-based learning. Available data include air and ground temperatures, precipitation, wind speed and direction, and solar radiation. These data can be easily accessed at the Emigrant Pass Observatory web site (http://thermal.gg.utah.edu/facilities/epo/). We suggest using a pretest of a student's knowledge and understanding of physical processes as a springboard to "jump in" and examine the EPO data, thus investigating the process as opposed to finding an answer.

References

American Association for the Advancement of Science, 1990, Science for all Americans: New York, Oxford University Press, 272 p.

Bartlett, M.G., D.S. Chapman, and R.N. Harris, 2006, A decade of ground-air temperature tracking at Emigrant Pass Observatory, Utah: J. Climate, 19, 3,722 - 3,731.

Brey, J.A., 2000, Assessing the use of real-time DataStreme weather data in an introductory physical geography course: Journal of Geography in Higher Education, v. 24, 116 – 122.

Brohan, P., J.J. Kennedy, I. Harris, S.F.B. Tett and P.D. Jones, 2006, Uncertainty estimates in regional and global observed temperature changes: a new dataset from 1850: J. Geophys. Res., 111, D12106, doi:10.1029/2005JD006548.

Chapman, D.S., and M.G. Davis, 2010, Climate Change: Past, Present, and Future: Eos Transactions of the American Geophysical Union, v. 91 (37), 325 – 326.

Davis, M.G., D.S. Chapman, and R.N. Harris, 2011, Geothermal record of climate change: in H. K. Gupta (Ed.), Encyclopedia of Solid Earth Geophysics; Springer Science, doi:10.1007/978-90-481-8702-7.

Davis, M.G., R.N. Harris, and D.S. Chapman, 2010, Repeat temperature measurements in boreholes from northwestern Utah link ground and air temperature changes at the decadal time scale: J. Geophys. Res., doi:10.1029/2009JB006875.

Hansen, J., R. Ruedy, M. Sato, and K. Lo, 2010, Global surface temperature change: Rev. Geophys., 48, RG4004, doi:10.1029/2010RG000345.

Hays, J.D., S. Pfirman, B. Blumenthal, K. Kasten, and W. Menke, 2000, Earth science instruction with digital data: Computers & Geosciences, v. 26, 657-668.

IPCC, 2007, Climate Change 2007: The Physical Science Basis. Contribution of Working Group I to the Fourth Assessment Report of the Intergovernmental Panel on Climate Change [Solomon, S., D. Qin, M. Manning, Z. Chen, M. Marquis, K.B. Averyt, M. Tignor and H.L. Miller (eds.)]. Cambridge University Press, Cambridge, United Kingdom and New York, NY, USA, 996 pp.

Martin, E.E., and P.D. Howell, 2001, Active inquiry, web-based oceanography exercises: Journal of Geoscience Education, v. 49, no. 2, 158 – 165.

Newell, B.R., and A.J. Pitman, 2010, The Psychology of Global Warming: Bulletin of the American Meteorological Society, 91, 1003 – 1014, doi:10.1175/2010BAMS2957.1.

National Research Council, 2011, Promising Practices in Undergraduate Science, Technology, Engineering, and Mathematics Education: Summary of Two Workshops, Natalie Nielsen, Rapporteur, Planning Committee on Evidence on Selected Innovations in Undergraduate STEM Education, Board on Science Education, Division of Behavioral and Social Sciences and Education, Washington, DC, The National Academies Press.

National Science Foundation, 1996, Shaping the future: New expectations for undergraduate education in science, mathematics, engineering, and technology: NSF 96-139, 76 p.

Putnam, S.N., and D.S. Chapman, 1996, A geothermal climate change observatory: First year results from Emigrant Pass in northwest Utah: J. Geophys. Res., 101, 21,877 - 21,890.

Roberts, D., E. Bradley, R. Keely, T. Eckmann, and C. Still, 2010, Linking Physical Geography Education and Research Through the Development of an Environmental

Sensing Network and Project-Based Learning: Journal of Geoscience Education, v. 58, no. 5, 262 – 274.

Smith, T.M., and R.W. Reynolds, 2005, A global merged land and sea surface temperature reconstruction based on historical observations (1880–1997): J. Clim., 18, 2021–2036.

Underwood, J., H. Smith, R. Luckin, and G. Fitzpatrick, 2008, E-Science in the classroom - towards viability: Computers & Education, v. 50, 535-546.